AJS American Journal of Science
publishing earth-sciences research since 1818

Saintilan, N. J., Ikenne, M., Bernasconi, S. M., Toma, J., Creaser, R. A., Souhassou, M., Allaz, J. M., Karfal, A., Maacha, L., & Spangenberg, J. E. (2023). The World's Highest-Grade Cobalt Mineralization at Bou Azzer Associated With Gondwana Supercontinent Breakup, Serpentinite and Kellwasser Hydrocarbon Source Rocks. *American Journal of Science*, *323*, 12. https://doi.org/10.2475/001c.91400

Science Paper

The World's Highest-Grade Cobalt Mineralization at Bou Azzer Associated With Gondwana Supercontinent Breakup, Serpentinite and Kellwasser Hydrocarbon Source Rocks

Nicolas J. Saintilan[1][a], Moha Ikenne[2], Stefano M. Bernasconi[3], Jonathan Toma[4], Robert A. Creaser[4], Mustafa Souhassou[5], Julien M. Allaz[1], Abdelaq Karfal[6], Lhou Maacha[6], Jorge E. Spangenberg[7]

[1] Institute of Geochemistry and Petrology, ETH Zürich, [2] LAGAGE, Faculty of Sciences, Ibn Zohr University, [3] Geological Institute, ETH Zürich, [4] Department of Earth and Atmospheric Sciences, University of Alberta, [5] EGERNE, Polydisciplinary Faculty of Taroundant, Ibn Zohr University, [6] CTT – Bou-Azzer mine – Managem Group, Twin Center – Tour A, [7] Institute of Earth Surface Dynamics, University of Lausanne

Keywords: Cobalt, arsenide, Bou Azzer, Gondwana, supercontinent, Kellwasser, serpentinite, sulfide Re-Os geochronology

https://doi.org/10.2475/001c.91400

American Journal of Science

Vol. 323, 2023

Cobalt arsenide deposits associated with Neoproterozoic serpentinite in Morocco represent the highest-grade cobalt resource worldwide. Yet, genetic models for their origin remain controversial. We report here mineralogical and geochemical evidence for arsenide-calcite mineralization at Bou Azzer to constrain the temporal framework and identify the geodynamic trigger for mineralization mechanisms. To this end, radiometric ages for ore minerals are paramount for understanding the origin of the Bou Azzer cobalt arsenide deposit. New safflorite ($CoAs_2$) rhenium-osmium (Re-Os) ages are Late Devonian in age: 380.4 ± 2.9 and 373.4 ± 1.2 to 368.1 ± 5.0 million years ago (Ma) for coarse-grained and fine-grained safflorite, respectively. These dates overlap with the timing of break-up of the supercontinent Gondwana, and the building of an arch-and-basin geometry from northern Africa to Arabia. Our findings temporally and spatially contextualize previous knowledge of fluid chemistry and mineralization mechanisms involving a two-fluid mixing. Arsenide mineralization resulted from mixing of a methane-dominated fluid with highly saline basinal brines that leached Os ($^{187}Os/^{188}Os_{initial}$ = 0.120 ± 0.001), and by corollary cobalt, from Neoproterozoic serpentinite. Carbon and sulfur stable isotope data of ore-stage calcite and arsenides, respectively, show that hydrocarbons acted as the main reductant for mineralization. We speculate that the seawater-derived brines sank into the sedimentary basins adjacent to a carbonate platform with the Bou Azzer serpentinite in its basement in the Late Devonian. In the context of an enhanced geothermal gradient, such brines would have been involved in warm hydrothermal alteration of hydrocarbon source rocks of the local expression of the Kellwasser event in the geological record of present-day Morocco. This warm hydrothermal alteration of hydrocarbon source rocks may have taken place for coarse-grained safflorite mineralization (380.4 ± 2.9 Ma) shortly after *ca.* 382–381 Ma Lower Kellwasser horizons were deposited, or, for fine-grained safflorite mineralization (373.4 ± 1.2 to 368.1 ± 5.0 Ma) while the Upper Kellwasser horizons of present-day Morocco were being deposited.

1. INTRODUCTION

Cobalt (Co) is a crucial element for metallurgical applications (e.g., specialty steels, jet engines) and the production of rechargeable lithium-ion batteries designed to face the needs of a transition to a low-carbon economy and ambitions of space exploration (Horn et al., 2021; Petavratzi et al., 2019). Whereas 66% of the global mine production of cobalt in 2018 came as a by-product from moderate-size to giant sedimentary rock-hosted copper sulfide deposits in Central Africa (0.03–1.08% Co; Petavratzi et al., 2019), the high-grade, lens-and-vein-type Bou Azzer deposit in Morocco remains the only major orebody in the world where cobalt is exploited as the main commodity (fig. 1A, 1B, *ca.* 120,000 metric tons per year, 1% Co; Petavratzi et al., 2019). Yet, the origin of such a Co resource comprising arsenide minerals (e.g., safflorite – $CoAs_2$, 21.25 weight percent [wt.%] Co; skutterudite – $CoAs_3$, 17.95 wt.% Co) remains highly debated given controversial genetic mod-

a Corresponding author: nicolas.saintilan@erdw.ethz.ch

els. Published evidence from mineralogy, mineral chemistry, and fluid inclusion microthermometry and chemistry (Ahmed et al., 2009; En-Naciri et al., 1997; Essarraj et al., 2005; Leblanc & Billaud, 1982) were reconciled in a general model for Bou Azzer-type mineralization. This model involves the dynamic and fast reduction of arsenic- and cobalt-nickel-iron-(Co-Ni-Fe)-bearing hydrothermal fluids, and controls exerted by pH variations on mineral precipitation and on the extent of Co-Ni endowment (Markl et al., 2016). However, the timing of arsenide mineralization and geodynamic setting for ore genesis remain unresolved but are paramount for a consensus on the secular distribution of Bou Azzer-type Co resources in Earth history.

The Bou Azzer Co-Ni arsenide orebodies are located in the Bou Azzer-El Graara window ('i.e.', "inlier") that forms part of the Anti-Atlas Pan-African orogenic belt (fig. 1A; Gasquet et al., 2005). The inlier, which was thrust onto the Paleoproterozoic West African Craton, represents a fragment of Tonian (*ca.* 759 million years ago, Ma) serpentinized oceanic lithosphere and Tonian to Cryogenian (*ca.* 760 to 690 Ma) intra-oceanic arc lithologies intruded by Cryogenian quartz diorite (*ca.* 660 Ma; Hodel et al., 2020; Triantafyllou et al., 2018). Elongated lenses of Co-Ni-Fe arsenides and their carbonate ± quartz envelopes (fig. 2A) are hosted in steep fault zones between serpentinite and diorite (fig. 1C, 2B), whereas Co-Ni-Fe arsenides vein systems occur within serpentinite and diorite (fig. 2C, 2D; Tourneur et al., 2021). Previous age estimates for the timing of arsenide mineralization have ranged from late Pan-African (~ 685–580 Ma; Leblanc, 1981) to late Variscan (*ca.* 310 Ma) on the basis of samarium-neodymium (Sm-Nd) geochronology of bulk calcite envelope and *in situ* uranium-lead geochronology of brannerite (UTi_2O_6) inclusions in calcite (Oberthür et al., 2009). Complex mineralizing processes have been invoked to explain the presence of calcite with different initial $^{143}Nd/^{144}Nd$ values. Therefore, it cannot be excluded that the *ca.* 308 Ma date of calcite may signal a rejuvenation of the Sm-Nd systematics in calcite (Oberthür et al., 2009). Scanning-electron microscope imaging combined with major- and trace-element microprobe analyzes of brannerite at Bou Azzer reveals that this mineral is internally inhomogeneous (Oberthür et al., 2009). Inhomogeneous brannerite (Oberthür et al., 2009) may result from the dissolution and/or reprecipitation of an earlier phase of uraninite (Ikenne et al., 2021; Johnson & Cross, 1995; Macmillan et al., 2017; Oberthür et al., 2009). These observations call therefore for caution when interpreting the *ca.* 310 Ma date of brannerite associated with Co mineralization at Bou Azzer (Ikenne et al., 2021). Younger Triassic dates have also been proposed based on the argon-argon ($^{40}Ar/^{39}Ar$) thermochronometer in adularia, which is associated with sulfide and sulfosalt deposits that occur throughout the central and eastern Anti-Atlas and is interpreted as being paragenetically late with respect to arsenide ores at Bou Azzer (Levresse, 2001). However, $^{40}Ar/^{39}Ar$ ages in adularia are readily thermally reset (see Chiaradia et al., 2013). To end with, preliminary evidence from rhenium-osmium (Re-Os) dates of molybdenite at Bou Azzer imply a major ore-forming event for Co-Ni-arsenide mineralization in the Late Devonian (Stein et al., 2021). Due to this age uncertainty and the lack of direct radiometric dates on ore minerals, the geodynamic context that contributed the bulk of Co mineralization in these rich deposits has remained an open question.

To provide a genetic model for epigenetic Co-arsenide mineralization related to hydrothermal, metal-bearing fluids, there are four key components to document: (1) source(s) of metals; (2) origin of the reducing agent to fix metals as arsenides; (3) the type and chemical composition of hydrothermal, metal-bearing fluids, and (4) the geodynamic engine that put hydrothermal fluids into motion through the source towards the trap site for mineralization. Without absolute radiometric dates of the ore arsenide minerals, we lack a temporal framework to evaluate possible geodynamic triggers. In turn, without knowing the trigger, we cannot evaluate mineralization mechanisms. Therefore, the provision of radiometric ages for ore minerals is paramount for understanding the origin of the Bou Azzer Co-arsenide deposit. Here, we present new high-precision Re-Os ages for safflorite that reveal a primary introduction of bulk Co mineralization at the time of dislocation of the Anti-Atlas during tectonic subsidence controlled by normal faulting throughout the northern edge of the supercontinent Gondwana in the Late Devonian. Combining these age constraints with new sulfur stable isotope data for arsenides, and carbon and oxygen clumped isotope data on the calcite envelope surrounding the ore confirms a link between Co mineralization and oil field brines as proposed in previous petrographic and fluid inclusion microthermometry studies (En-Naciri et al., 1997; Essarraj et al., 2005). Further, these geochemical and geochronological data reveal that the Late Devonian rifting and mantle exhumation responsible for the well-known arch-and-basin geometry present from northern Africa to Arabia (Frizon de Lamotte et al., 2013), also triggered the formation of the highest-grade cobalt ore deposit known on Earth.

2. MATERIAL AND METHODS

2.1. Petrography and preparation of monophasic sulfide mineral separates

Four safflorite-mineralized samples from the Co-Ni-arsenide mineral deposit at Aït Ahmane, Bou Azzer district, Morocco were taken from the mineralized open pits F53 and F55 (fig. 1C & table S1). The paragenetic sequence between safflorite and calcite was established based on macroscopic descriptions and petrographical observations of polished thin sections using transmitted and reflected light microscopy (fig. 2A). These timing relationships constrained the workflow for optimum mineral separation of safflorite into monophase mineral separates according to the protocol presented in Saintilan et al. (2020a). This workflow is based on a first step of heavy liquid separation to isolate the bulk analyte (70–200 mesh sizes), followed by magnetic separation (I = 1.5 A) using a Frantz Isodynamic Separator to produce a safflorite final mineral separate in the non-magnetic fraction. Quality control of the mineral separates

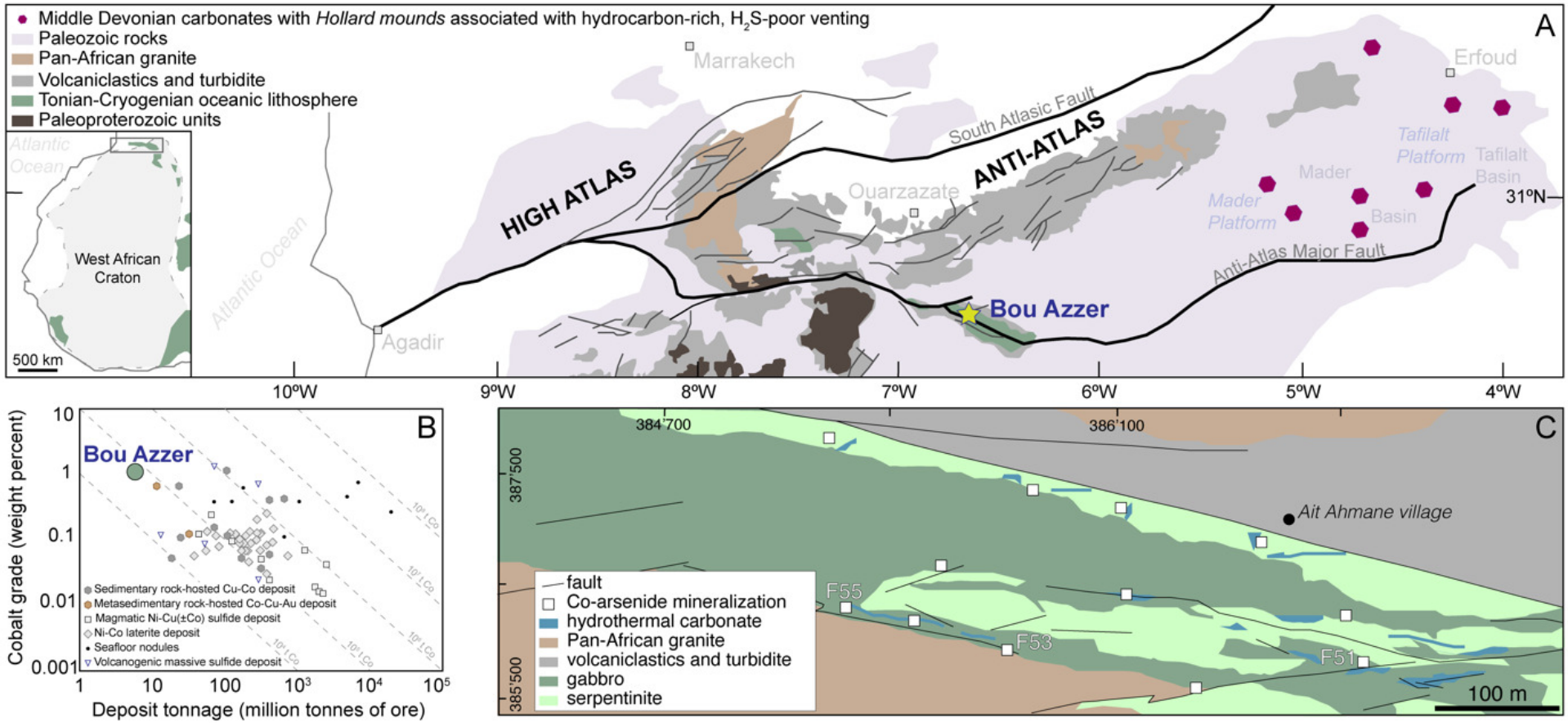

Figure 1. Regional geology, field relationships and economical aspects of Bou Azzer nickel-cobalt (Ni-Co) arsenide deposit, Central Anti-Atlas, Morocco.

A Regional geological map of Anti-Atlas and location of Bou Azzer deposit in the Bou Azzer-El Graara window (after Hodel et al., 2017, 2020). **B** Grade versus tonnage diagram showing high-grade, low-tonnage Bou Azzer deposit in comparison with data for other major cobalt producing metallogenic provinces and deposit types (after Petavratzi et al., 2019). **C** Local geological map around the Aït Ahmane area in the central Bou Azzer district (after Ez-Zghoudy et al., 2023; coordinates in Lambert South Reference). The location of the pits in which Co-arsenide mineralization is exploited is shown. The Co-arsenide- and/or hydrothermal calcite-mineralized samples (table S1) utilized in the present study come from pits F51, F53 and F55.

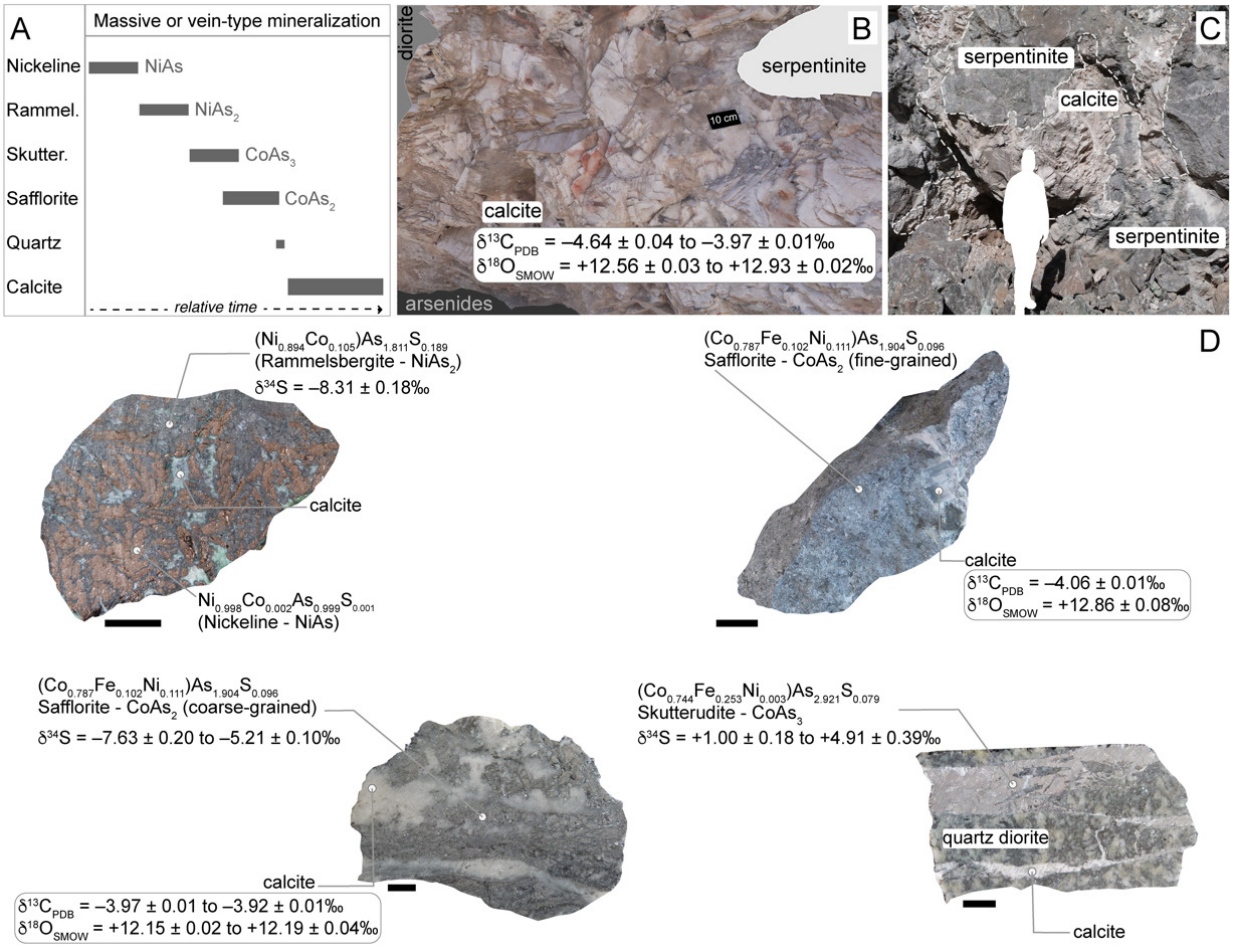

Figure 2. Paragenetic sequence, field relationships and ore mineralogy at Bou Azzer.

A Paragenetic sequence of Ni-Co-arsenides and gangue minerals at Bou Azzer based on the studied samples. Abbreviations: Rammel.: rammelsbergite; Skutter: Skutterudite. **B** Local field relationships of arsenide-mineralized zones and calcite envelopes with respect to Tonian serpentinite and Cryogenian diorite. **C** Arsenide-mineralized samples utilized in the present study (all scale bars are 1 cm long). These samples display the systematic occurrence of Co- and/or Ni-arsenides with calcite. Additional geographical, petrographical and geochemical data for the samples can be found in tables S1 & S2. Mineral chemical data are reported in table S7.

was conducted according to the method of Saintilan et al. (2020a).

2.2. Arsenide major and minor element chemistry

Quantitative microanalyses were obtained on a JEOL JXA-8230 electron microprobe at the Institute of Geochemistry and Petrology, ETH Zürich, Switzerland. This is a five-spectrometer instrument equipped with argon X-ray detectors (P-10 mixture) on spectrometers 1, 2, and 5, and xenon X-ray detectors on spectrometers 3 and 4. Analytical conditions were 15 kV and 50 nA with a 5 µm beam diameter. All analyzes were acquired using the software Probe for EPMA. Background measurements were done at interference-free spectrometer positions. Details of the element setup and standards used are listed in table S5. To improve the accuracy of some minor and trace element analyzes in arsenide, the shared background acquisition of Allaz et al. (2019) was applied. Counting times were optimized to improve detection limits while keeping analysis time reasonable at *ca.* 2 minutes per point. The ZAF matrix correction from Armstrong (1988) using the FFAST mass absorption coefficient table (Chantler et al., 2005) was applied throughout. Typical detection limits are on the order of 0.01 to 0.03 wt% for most elements (table S6). Major and minor element analyzes by electron microprobe were used to calculate atomic proportions and corresponding mineral formulae of arsenides.

2.3. Rhenium-osmium radiogenic isotope geochemistry of safflorite

For each analysis, between 269 and 440 mg of safflorite mineral separates were weighed and transferred into thick-walled borosilicate Carius tubes (Shirey & Walker, 1995). Each sulfide aliquot was dissolved in inverse Aqua Regia (~3 mL of 11N HCl and ~ 6 mL 16N HNO_3) with a known amount of "^{185}Re+^{190}Os spike" solution at 210ºC for 24 h (Laboratory of Rhenium-Osmium Isotope Geochemistry and Geochronology, Isotope Geochemistry and Cosmochemistry Group, Institute of Geochemistry and Petrology, ETH Zürich). The laboratory protocol used in the present

work is described in full details in Selby and Creaser (2001), Selby et al. (2009), Hnatyshin et al. (2016), and Li et al. (2017). In brief, Os was isolated and purified from the inverse Aqua Regia solution by chloroform ($CHCl_3$)-hydrobromic acid (HBr) solvent extraction at room temperature, and, by microdistillation (Birck et al., 1997; Cohen & Waters, 1996; Roy-Barman & Allègre, 1995; Selby & Creaser, 2001; Shen et al., 1996). The Re was isolated using an acetone-sodium hydroxide (Acetone-NaOH) step (Bozhkov et al., 1985; C. Li et al., 2009; Matthews & Riley, 1970), followed by HCl–HNO_3-based anion chromatography (Cumming et al., 2013; Morgan et al., 1991). The Re and Os isotopic compositions were determined by negative thermal ionization mass spectrometry (N-TIMS) using a Thermo Scientific Triton mass spectrometer at the Institute of Geochemistry and Petrology, ETH Zürich, Switzerland. Rhenium and Os were loaded onto outgassed Ni and Pt filaments, respectively. Rhenium was measured as ReO_4^- in static mode on Faraday collectors, whereas Os was measured as OsO_3^- in peak-hopping mode on a single electron multiplier (Creaser et al., 1991; Völkening et al., 1991). Measurement quality was monitored by repeated measurements of in-house standard solution for Re (125 pg aliquot – $^{185}Re/^{187}Re$ = 0.5986 ± 0.0005, 2σ, *n* = 22) and Os (Durham Romil Os Standard, DROsS; Nowell et al., 2008; 50 pg aliquot – $^{187}Os/^{188}Os$ = 0.16092 ± 0.00069, 2σ, *n* = 12). Rhenium analyses are (i) corrected for isobaric oxide interferences using our long-term measurements of our in-house standard Re solution and (ii) normalized to an accepted value of the natural $^{185}Re/^{187}Re$ ratio (0.5974; Gramlich et al., 1973). Raw OsO_3^- ratios are corrected using an exponential law for isobaric oxide interferences, spike contribution and mass fractionation using an accepted value of the $^{192}Os/^{188}Os$ ratio of 3.08261 (Creaser et al., 1991; Hnatyshin et al., 2016). Total procedural blank using inverse Aqua Regia was: (i) for batch RO-006, 1.55 ± 0.02 pg Re and 28 ± 2 fg Os with a blank $^{187}Os/^{188}Os$ isotope composition (IC) of 0.43 ± 0.08 (2σ, *n* = 2); (ii) for batches RO-008, RO-010 & RO-011, 3.27 ± 0.02 pg Re and 44 ± 2 fg Os with a blank $^{187}Os/^{188}Os$ IC of 0.43 ± 0.09 (2σ, *n* = 3); (iii) for batch RO-009, 2.23 ± 0.01 pg Re and 113 ± 11 fg Os with a blank $^{187}Os/^{188}Os$ IC of 2.96 ± 0.92 (2σ, *n* = 1). The analytical uncertainties result from full error propagation of weighing errors, standard measurements, mass spectrometry analyzes and blanks. The Re-Os data for sarflorite are plotted in the $^{187}Os/^{188}Os$ vs. $^{187}Re/^{188}Os$ space with the error correlation value (*rho*; Ludwig, 1980) and the 2σ calculated uncertainties for the $^{187}Os/^{188}Os$ and $^{187}Re/^{188}Os$ values (fig. 3A). An isochron date is calculated using IsoplotR (Vermeesch, 2018). Total uncertainty on the Re-Os dates is presented with and without including the decay constant λ of ^{187}Re as determined by Smoliar et al. (1996; λ = $1.666e^{-11}$ ± $5.165e^{-14}$ a^{-1}, 2σ).

For samples BAZ-14 & BAZ-15, preliminary analyzes using dissolution with a known amount of "^{185}Re+^{190}Os spike" solution showed an Os budget dominated by radiogenic ^{187}Os* and lacking common Os. Therefore, new analyzes of each sulfide aliquot were performed by using the same protocol as above but with a known amount of "^{185}Re+^{188}Os+^{190}Os spike" solution at 220°C for 48 h. The Re and Os isotopic compositions were determined by N-TIMS using a Thermo Scientific Triton Plus mass spectrometer at the Canadian Centre for Micro-Analysis, Department of Earth and Atmospheric Sciences, University of Alberta, Canada. Measurement quality was monitored by measurements of in-house Re and Os standards over the analysis period ($^{185}Re/^{187}Re$ = 0.59775 ± 0.00042, *n* = 8; AB-2 Os Standard, $^{187}Os/^{188}Os$ = 0.10689 ± 0.00061 1SD, *n* = 14). An average total procedural blank of 3.0 ± 0.3 pg Re and 44 ± 33 fg Os with a blank $^{187}Os/^{188}Os$ ratio of 0.30 ± 0.06 (*n* = 3) was measured over the duration of the safflorite analyzes. Reference Material 8599 Henderson molybdenite (Wise & Watters, 2011) was routinely analyzed as an age standard with the "^{185}Re+^{188}Os+^{190}Os spike". During the past 8 years, this reference sample has returned an average Re-Os date of 27.68 ± 0.07 Ma (*n* = 37), indistinguishable from the reported reference age of 27.66 ± 0.02 Ma (Markey et al., 2007). Individual model ages *t* for each safflorite aliquot are calculated using equation (1):

$$t = \left(\frac{1}{\lambda}\right) \cdot ln(^{187}\frac{Os^*}{^{187}Re} + 1) \quad (1)$$

2.4. Sulfur stable isotope geochemistry

Sulfur isotope geochemistry was carried out at the Institute of Earth Surface Dynamics, University of Lausanne, Switzerland. Based on microprobe analysis, only rammelsbergite, safflorite and skutterudite have sulfur contents greater than 0.03 wt.%. In addition to the safflorite mineral separates used for Re-Os isotope geochemistry, mineral separates of rammelsbergite and skutterudite were produced by following and modifying where necessary the protocol by Saintilan et al. (2020a). About 15 to 40 mg of pure nickeline, safflorite and skutterudite mineral separates were powdered in a hand-held agate mortar and pestle. Arsenide aliquots were analyzed by the new protocol of Spangenberg et al. (2022) for sulfur (S) concentration and sulfur stable isotope composition. Standards distributed by the International Atomic Energy Agency (IAEA-S_1, -S_2, and -S_3) were analyzed for calibration. Repeated measurements of these standards gave reproducibility better than 0.14‰. Data are reported in $\delta^{34}S$ notation as per mil (‰) variations from the Vienna Cañon Diablo Troilite (V-CDT) standard.

2.5. Carbon, oxygen, and clumped isotope geochemistry

A meter-size calcite block was collected *in situ* from the envelope of calcite at the contact between serpentinite and diorite in the vicinity of Ni ± Co-arsenide concentrations (fig. 2B) in open pit F51 (Aït Ahmane deposit, Bou Azzer district, fig. 1C). This block was cut into four sub-samples (samples BAZ-01a, b, c, d). In addition, pluricentimetric calcite crystals were extracted with tweezers from hand samples of fine-grained (BAZ-10, open pit F55) or coarse-grained (BAZ-15, open pit F53) safflorite-bearing samples (fig. 2D) prior to production of arsenide mineral separates from those samples. An additional sample of calcite asso-

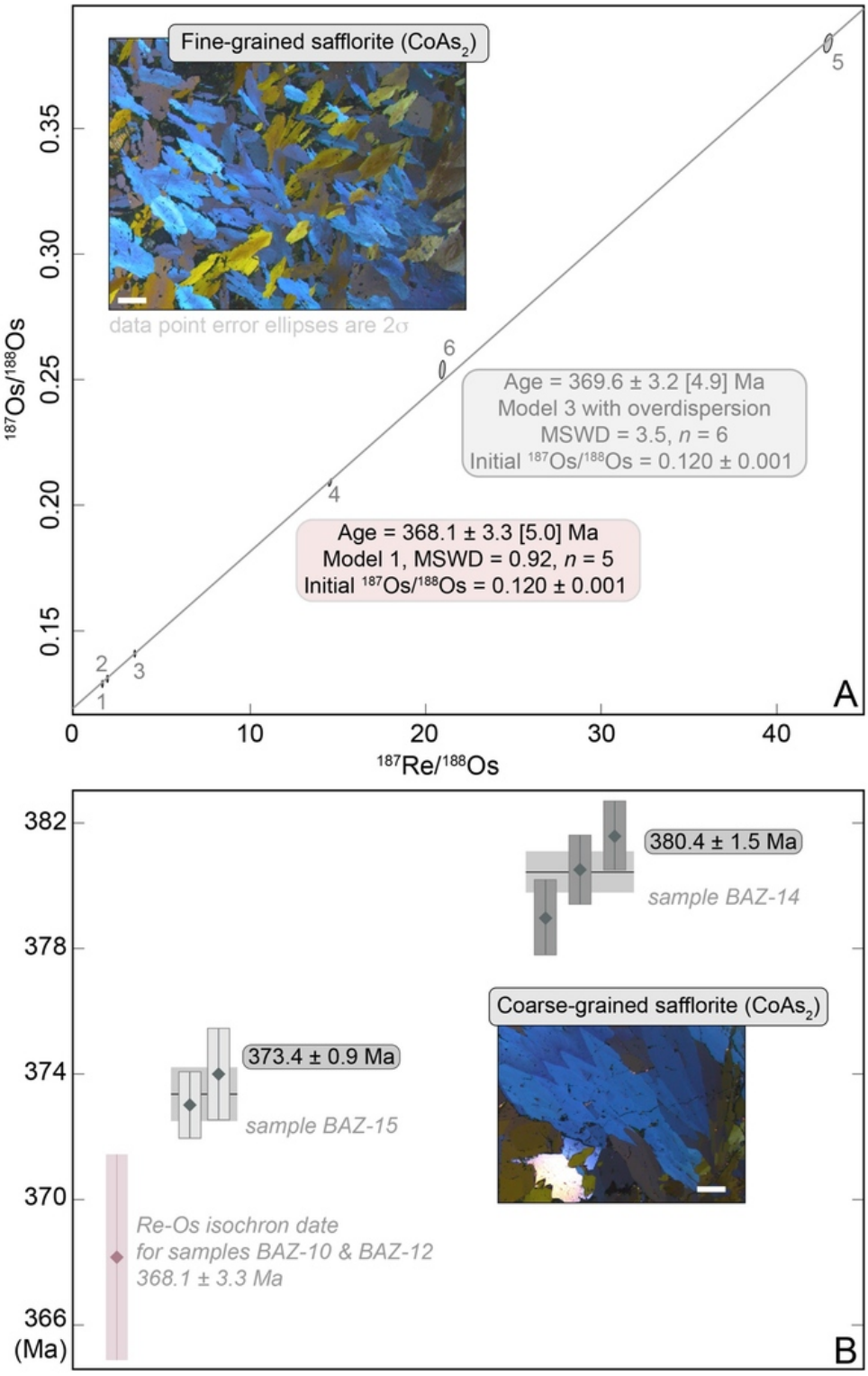

Figure 3. Rhenium-osmium geochronology of safflorite ($CoAs_2$) at Bou Azzer. Insets show reflected light microscopy images (crossed nicols) of material analyzed in each case (scale bars are 200 µm).

A Model 3 six-point & Model 1 five-point isochron regressions of data points for fine-grained safflorite in conventional $^{187}Os/^{188}Os$ vs. $^{187}Re/^{188}Os$ diagram (see text for details). Individual ellipses show 2σ uncertainty of each data point in $^{187}Os/^{188}Os$ vs. $^{187}Re/^{188}Os$ space. Ellipses are constructed from maximum and minimum error vectors that are orthogonal to each other. Maximum and minimum uncertainties are statistical values that are calculated from uncertainties of the $^{187}Os/^{188}Os$ and $^{187}Re/^{188}Os$ ratios for a given data point. Final uncertainties were calculated by full error propagation of uncertainties in the Re and Os measurements, blank values, isotopic compositions, and reproducibility of the standard Re and Os values. **B** Weighted mean of Re-Os model age (2σ, uncertainty of decay constant of ^{187}Re not included in the total uncertainty presented) and replicate(s) for coarse-grained safflorite bereft of or with low amounts of common Os. All Re-Os isotope data can be found in table S4. The Re-Os isochron date for fine-grained safflorite presented in fig. 3A is shown for comparison.

ciated with coarse-grained safflorite was collected (BAZ-17, open pit F53). Individual calcite samples were powdered in a hand-held agate mortar and pestle to obtain at least 1g of final powdered product.

The carbon, oxygen, and clumped isotope compositions of carbonates were determined at ETH Zürich using a Thermo Fisher Scientific 253Plus mass spectrometer coupled to a Kiel IV carbonate preparation device, following the methods described in Schmid and Bernasconi (2010), Meckler et al. (2014), and Müller et al. (2017). The Kiel IV device includes a custom built PoraPakQ trap held a −40 °C to eliminate potential organic contaminants. Prior to each sample run, the pressure-dependent backgrounds were determined on all beams to correct for non-linearity effects in the mass spectrometer. During each run, 22 replicates of 90–110 µg of different samples and five replicates of each carbonate standards, ETH-1, ETH-2, and 10 replicates of ETH-3, were analyzed for data normalization. Two replicates of the international standard, IAEA C2, were analyzed to monitor the long-term reproducibility of the method. All instrumental and data corrections are carried out with the software Easotope (John & Bowen, 2016) using the revised IUPAC parameters for ^{17}O correction (Daëron et al., 2016). Results are presented in the I-CDES (Intercarb Carbon Dioxide Equilibration Scale) according to Bernasconi et al. (2021). Temperatures are calculated using the N. T. Anderson et al. (2021) universal calibration.

3. RESULTS

3.1. Mineralogy, mineral chemistry, and sulfur stable isotope composition of arsenides

Arsenide deposits with meter-scale envelopes of calcite are mostly located at the contact between serpentinite and intrusive Pan-African diorite (figs. 1C, 2B). The arsenide mineralization occurs also as localized and mineral-specific replacements (e.g., magnetite; Tourneur et al., 2021) in brecciated blocks of serpentinite cemented by calcite (fig. 2C). In the studied samples, skutterudite (Co tri-arsenide) is only found in anastomosing veins with accessory calcite within brittle structures in diorite (fig. 2D). Nickeline, which initiates the paragenetic sequence (fig. 2A, 2D), is bereft of sulfur and has a stoichiometric composition (fig. 2D). In contrast, the Ni di-arsenide rammelsbergite (fig. 2D) forms a solid solution with the Co di-arsenide safflorite with an average of 10.5% Co substituting for Ni (table S2). Rammelsbergite contains 1.63 ± 0.30 wt.% S (2 standard errors – SE) and has the lowest $\delta^{34}S$ values among the analyzed arsenides (−8.31 ± 0.18‰, 2SE; table S3). The sulfur contents in safflorite lie between 1.18 ± 0.47 and 2.25 ± 0.49 wt.% S with similarly low $\delta^{34}S$ values of −7.63 ± 0.20 to −5.21 ± 0.10‰. Safflorite (fig. 2D), which contains an average of 10.2% Fe and 11.1% Ni substituting for Co, forms a solid solution with the iron (Fe) di-arsenide löllingite, in addition to rammelsbergite. Skutterudite, with an average of 25% Fe substituting for Co, stands out as the arsenide species least enriched in sulfur (0.31 ± 0.13 to 0.65 ± 0.54 wt.% S) and with distinct positive $\delta^{34}S$ values (+1.00 ± 0.18 to +4.91 ± 0.39‰).

3.2. Mineral-specific rhenium-osmium geochronological constraints on mineralization

The Re-Os data for fine-grained safflorite yield a Model 3 date of 369.6 ± 3.2 [4.9] Ma [bracketed uncertainty includes the 0.31% uncertainty in the decay constant of ^{187}Re; n = 6; mean square of weighted deviates (MSWD) = 3.5; 2σ; initial $^{187}Os/^{188}Os$ ratio – Os_i, 0.120 ± 0.001; fig. 3A and table S4]. A Model 3 isochron regression includes a measure of overdispersion attributed to geological uncertainty in the value for Os_i, 'i.e.', all aliquots may not have the same Os_i within the uncertainty of a Model 1 regression (Vermeesch, 2018). A Model 1 inverse isochron regression (not shown; Y. Li & Vermeesch, 2021) shows that analytical point 6 in figure 3A is a statistical outlier. Thus, a Model 1 isochron regression on the other 5 data points (MSWD = 0.92) yields a date of 368.1 ± 3.3 [5.0] Ma with an Os_i at 0.120 ± 0.001. The Re-Os isochron age results of 368.1 ± 3.3 Ma (Model 1, n = 5) vs. 369.6 ± 3.2 Ma (Model 3, n = 6) does not change the interpretations and conclusions that mineralization is Late Devonian in age. In contrast, coarse-grained safflorite (sample BAZ-15), which is bereft of common Os (≤0.1 pg common Os), yields model ages that replicate with a weighted mean average of 373.4 ± 0.9 [1.2] (n = 2, fig. 3B; table S4). Coarse-grained safflorite (sample BAZ-14), which has low amounts of common Os (6.8–16.1 pg common Os) in comparison to radiogenic ^{187}Os contents (2.13–2.24 ppb ^{187}Os), yields model ages of *ca.* 380 Ma with a weighted average of 380.4 ± 1.5 [2.9] (n = 3, fig. 3B; table S4).

The three distinct Re-Os date groupings indicate at least three episodes of safflorite mineralization spanning *ca.* 12.8 ± 3.4 million years. We suggest that these dates reflect discrete episodes of mineralization, rather than resetting or disturbance of the Re-Os geochronometer in safflorite. We base this reasoning on independent and empirical evidence for the Re-Os system in sulfarsenides (arsenopyrite FeAsS and its solid solution with cobaltite – CoAsS – and gersdorffite – NiAsS; Davies et al., 2010; Majzlan et al., 2022; Morelli et al., 2010; Saintilan, Creaser, & Bookstrom, 2017; Saintilan, Creaser, Spry, et al., 2017; Saintilan et al., 2020b) and one arsenide (löllingite $FeAs_2$; Saintilan, Creaser, Spry, et al., 2017). The robustness of the mature Re-Os arsenopyrite geochronometer was demonstrated in case studies against independent U-Pb age constraints on zircon or monazite (e.g., Davies et al., 2010; Morelli et al., 2010; Saintilan, Creaser, Spry, et al., 2017; Saintilan et al., 2020b; Scherstén et al., 2012). For arsenopyrite, closure temperature of the Re-Os system was constrained at *ca.* 600 °C (e.g., Davies et al., 2010; Morelli et al., 2010; Rooney et al., in press; Saintilan, Creaser, Spry, et al., 2017; Saintilan et al., 2020b). Further, Saintilan, Creaser, Spry and Hnatyshin (2017) in their study of the Re-Os chronometer in arsenopyrite weighed against independent monazite U-Pb age constraints concluded on the robustness of the löllingite Re-Os geochronometer with closure temperature between 550 and 600 °C. Given that löllingite ($FeAs_2$) forms a solid solution with safflorite ($CoAs_2$), we targeted saf-

florite at Bou Azzer for Re-Os isotope geochemistry and geochronology, assuming similar closure temperatures as for löllingite (i.e., 550 to 600 °C).

The aspects of diffusion of Os have only been studied in molybdenite (Selby & Creaser, 2004; Stein et al., 2003) and in pyrite and pyrrhotite (Brenan et al., 2000). For sulfarsenides and arsenides, such knowledge is not yet available and as such, direct calculation of a closure temperature for safflorite is not possible. The most robust mineral for Re-Os dating is molybdenite (Selby & Creaser, 2001; Stein et al., 2001; Takahashi et al., 2007). At Bou Azzer, a range of recently reported molybdenite dates indicates a major ore-forming event in the Late Devonian (Stein et al., 2021) closely matching our arsenide ages. Thus, we suggest that the safflorite Re-Os dates in the present work are not recording resetting by Os diffusion or recrystallization effects.

3.3. Clumped and carbon-oxygen stable isotope composition of ore-stage calcite

To complement previous evidence that mineralizing fluids were derived from heated seawater-derived brines (En-Naciri et al., 1997; Essarraj et al., 2005) and place new geochemical constraints on the redox conditions for mineralization, powdered calcite aliquots (n = 66) from eight samples were analyzed for carbon and oxygen isotope composition ($\delta^{13}C$ in ‰ VPDB and $\delta^{18}O$ in ‰ VSMOW; fig. 4) and clumped isotopes (I-CDES, table S5). The $\delta^{18}O_{fluid}$ values of the hydrothermal fluid in equilibrium with calcite are calculated according to the calibration of O'Neil et al. (1969). Calcite at the contact between serpentinite and diorite has low $\delta^{13}C$ values (−4.64 ± 0.04 to −3.97 ± 0.02‰, 1 standard deviation – SD). Its clumped isotope data (Δ_{47} = 0.350 ± 0.006 to 0.375 ± 0.006‰, 1 standard error – SE) and $\delta^{18}O$ values (+12.57 ± 0.03 to 12.93 ± 0.05‰) signal a minimum average temperature of the hydrothermal fluid ($T_{min\text{-}fluid}$) of 146 to 172 °C and $\delta^{18}O_{fluid}$ at −0.34 to +1.90‰. Calcite intergrown with safflorite has similarly low $\delta^{13}C$ values (−4.06 ± 0.02 to −3.92 ± 0.01‰). The hydrothermal fluid at the root of this calcite associated with Co-arsenides has overall slightly higher $T_{min\text{-}fluid}$ (172–219 °C for Δ_{47} = 0.314 ± 0.021 to 0.349 ± 0.028‰) and slightly higher $\delta^{18}O_{fluid}$ of +1.26 to +3.72‰ (for $\delta^{18}O_{calcite}$ = +12.15 ± 0.02 to 12.86 ± 0.08‰).

4. DISCUSSION AND CONCLUSIONS

4.1. Geochronological implications and regional geodynamic context

Our new Re-Os ages constrain the timing of cobalt arsenide mineralization at Bou Azzer in the Late Devonian starting in the Frasnian at *ca.* 380.4 Ma until shortly after the Frasnian–Famennian boundary at *ca.* 373.4 to 368.1 Ma (figs. 3 & 5). These time stamps signal the primary introduction of bulk Co mineralization during dislocation of the Anti-Atlas in the Middle to Late Devonian, in connection with subsidence controlled by normal faulting that occurred throughout the northern edge of the Gondwana supercontinent (Wendt, 1985). This tectonic episode is part of a global event of rifting, mantle exhumation and thermal uplift that is responsible for the well-known arch-and-basin geometry that is recognized from present-day northern Africa to Arabia and is inherited from the breakup of northern Gondwana (Frizon de Lamotte et al., 2013).

In the Late Devonian, the central Anti-Atlas, including the Bou Azzer area, was a continental platform to major sedimentary basins located in the present-day eastern Anti-Atlas (Mader and Tafilalt Basins; fig. 1A; fig. 6). Hereafter, we refer to the carbonate-shale platform at Bou Azzer on the eastern edge of the Anti-Atlas as the "Bou Azzer platform". During the Middle to Late Devonian, the eastern edge of the Anti-Atlas (in particular, the Tafilalt basin & platform) underwent extensional tectonic activity. This tectonic activity is attested by sharp variations in sediment thickness and syn-sedimentary faulting (Pouclet et al., 2017; Wendt, 2021) which caused major transgressions during the Late Devonian with an increased frequency of syn-sedimentary fault movements (Wendt, 2021). This tectonic context is also contemporaneous with significant calc-alkaline magmatic activity (Franchi et al., 2015; Pouclet et al., 2017). Protracted sodic alkaline magmatism is attested in the Tafilalt Basin from the late Devonian (Famennian) to the end of the Lower Carboniferous (Tournaisian) (Pouclet et al., 2017). This geodynamic configuration has been interpreted as being related to a thermal anomaly and uplift associated with a mantle anomaly (Frizon de Lamotte et al., 2013). In the Tafilalt platform, this magmatic activity fueled the circulation of warm hydrothermal fluids within the overlying carbonate units (Franchi et al., 2015). Further, in the context of sustained syn-sedimentary faulting, the eastern edge of the Anti-Atlas and the Bou Azzer platform could have focused large quantities of hydrothermal fluid flow resulting in hydrothermal mineralization triggered by episodic and seismically induced fluid pulses (see Sibson et al., 1975).

Further to this, the timing of the mineralizing processes leading to the highest-grade Co ore deposit on Earth coincides with the two events comprising the Kellwasser episode (fig. 5) as illustrated by specific hydrocarbon source rocks in the sedimentary record in the eastern and central Anti-Atlas in the Mader-Tafilalt Basins and adjacent carbonate platforms (Wendt & Belka, 1991). The Bou Azzer pelagic platform comprised black bituminous limestone and shale (Wendt & Belka, 1991) above a basement that included the future loci of the Bou Azzer deposits at the tectonic contacts between Neoproterozoic serpentinite and Pan-African granodiorite (fig. 6). The hydrocarbon source rocks in the Bou Azzer platform may have been deposited in the context of a major biotic crisis, 'i.e.', the Kellwasser event (fig. 5; Carmichael et al., 2019; Hollard, 1974; Schindler, 1990; Wendt & Belka, 1991). The Late Devonian Kellwasser event was a series of modification of marine ecosystems of global scope with variable lithological and geochemical expressions depending on paleogeography and paleoenvironment (Carmichael et al., 2019). At its type locality (Steinbruch Schmidt outcrops, Germany; Devleeschouwer et al., 2002), the Kellwasser event is cali-

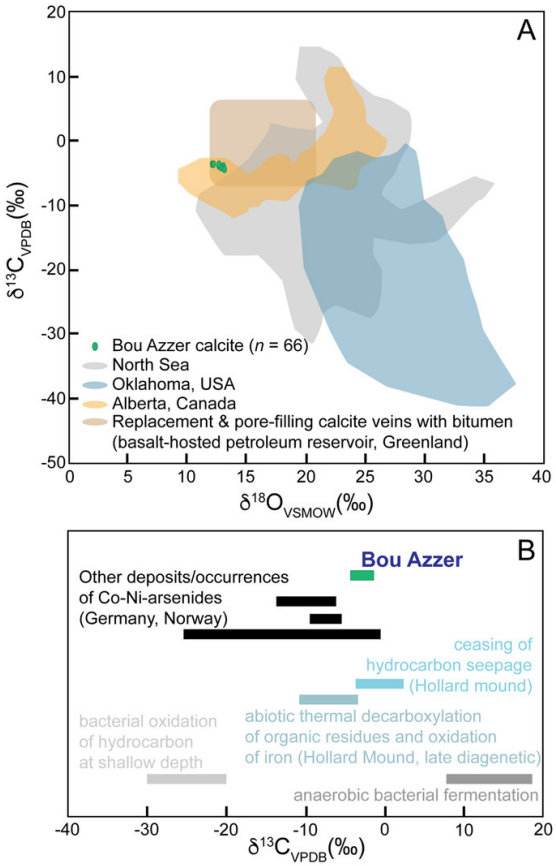

Figure 4. Genetic contextualization of stable isotope geochemical data for calcite associated with cobalt arsenide mineralization at Bou Azzer.

A $\delta^{13}C$ versus $\delta^{18}O$ diagram of Bou Azzer calcite compared to data for calcite in major sediment- or basalt-hosted petroleum reservoirs worldwide (data for calcite in petroleum reservoirs after Rogers et al., 2006 and references therein). The full data set of carbon and oxygen isotope data of calcite is found in table S5. **B** $\delta^{13}C$ isotope data for Bou Azzer calcite compared to empirical ranges of $\delta^{13}C$ isotope signatures of dissolved inorganic carbon resulting from abiotic and biotic processes involving degradation of hydrocarbons (after Irwin et al., 1977; Macaulay et al., 2000).

brated immediately prior the Frasnian-Famennian boundary at 371.86 ± 0.08 Ma and comprises two horizons above and below a bentonite layer (uranium-lead isotope dilution thermal ionization mass spectrometry zircon age of 372.36 ± 0.05 Ma; Percival et al., 2018; fig. 5) assigned to the Upper *rhenana* conodont Zone (Ziegler & Sandberg, 1990). In Morocco, the sedimentary record of potential Kellwasser anoxic horizons is not calibrated by absolute radiometric ages nor astrochronological correlations (fig. 5) as done for other Kellwasser sequences at the global scale (De Vleeschouwer et al., 2017; Percival et al., 2018). Current interpretations suggest that a first and short Lower Kellwasser episode at *ca.* 382 to 381 Ma (lowermost Frasnian, fig. 5; Wendt & Belka, 1991) preceded a longer Upper Kellwasser episode starting possibly at *ca.* 373 to 371 Ma across the Frasnian-Fammenian boundary. The Upper Kellwasser overlapped with the peak of extensional tectonics in the eastern Anti-Atlas during the late Frasnian to early Famennian (Wendt & Belka, 1991).

The two types of hydrocarbon source rocks in the Bou Azzer platform are known to be able to generate hydrocarbons involved in epigenetic sulfide mineralization related to hydrothermal, metal-bearing fluids derived from basinal brines (e.g., Laisvall sandstone-hosted sulfide deposit related to exogenous hydrocarbons generated from buried black shale, Saintilan et al., 2019; Saintilan, Spangenberg, Samankassou et al., 2016; Ruby Creek sulfide deposit in dolomitized carbonaceous limestone; Saintilan et al., 2023). In addition, carbonate-shale platforms are ideal loci for evaporative, seawater-derived brine factories adjacent to sedimentary basins (Leach et al., 2010; fig. 6). In the context of an increased geothermal gradient (Frizon de Lamotte et al., 2013; Pouclet et al., 2017), such brines were involved in the form of heated hydrothermal fluids (En-Naciri et al., 1997; Essarraj et al., 2005) in the episodic mineralizing processes at Bou Azzer as evidenced by our new safflorite Re-Os ages. These hydrothermal fluids had the appropriate salinity and temperatures (as shown by evidence from fluid inclusions microthermometry studies; En-Naciri et al., 1997; Essarraj et al., 2005) to leach cobalt and, to a lesser extent, nickel from serpentinite (see details of the nature of the mineralizing fluids and mineralizing mechanisms in the next section 4.2.). In addition, such brines sinking into and refluxing within the Mader and Tafilalt sedimentary basins adjacent to the Bou Azzer platform (fig. 1A) would have resurged episodically via seismically

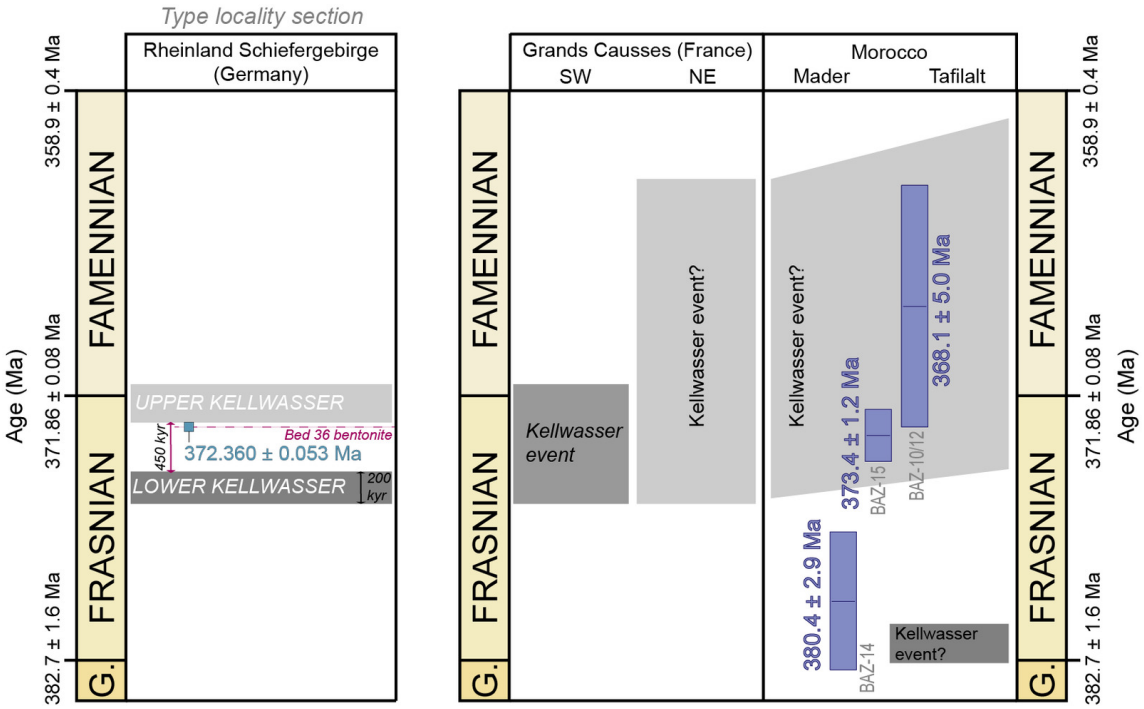

Figure 5. Comparison of the new Re-Os ages of safflorite at Bou Azzer with the assumed timing of the Kellwasser event in Morocco.

For reference, the chronological constraints from local absolute radiometric ages and global cyclostratigraphy of the Kellwasser events at its type locality at Steinbruch Schmidt, Rheinland Schiefergebirge, Germany, are shown. The dates of the Frasnian-Famennian boundary and the bentonite horizon bed 36 are after Percival et al. (2018). The duration of the Lower and Upper Kellwasser Events and their chronostratigraphic positions are after De Vleeschouwer et al. (2017). In other localities that were not included in the global correlations by De Vleeschouwer et al. (2017, e.g., Grands Causses, France; Mader and Tafilalt Basins, Morocco), the start, end, and duration of deposition of organic-rich sedimentary rocks (black shale and limestone) facies, supposedly representing the Lower and Upper Kellwasser Events, are much less well-constrained (after Wendt & Belka, 1991). The blue bars represent the three absolute Re-Os radiometric ages (including 2σ uncertainty with uncertainty in the decay constant of ^{187}Re) for safflorite in the Bou Azzer district presented in this study.

induced fluid pulses in the context of intense extensional activity in the Middle to Late Devonian (Pouclet et al., 2017; Wendt, 2021). Then, according to the general model of Markl et al. (2016) for Co-Ni-arsenide mineralization, we speculate these warm brines triggered hydrothermal alteration of hydrocarbon source rocks of the Kellwasser episode (fig. 6 and its inset) that were either deposited previously (*ca.* 382–381 Ma Lower Kellwasser event of Morocco, fig. 5) or were being deposited at the time of Co-arsenide mineralization (Upper Kellwasser event of Morocco, fig. 5).This hydrothermal alteration of hydrocarbon source rocks would have produced methane for episodic Co-arsenide mineralization at Bou Azzer (see details of mineralization mechanisms in the next section).

4.2. Origin of fluids and dynamics of fluid mixing

The wider geodynamic environment of extensional tectonics in the Late Devonian on the northern edge of Gondwana is compatible with deposit-scale fault patterns and petrographic observations documenting mineralization at Bou Azzer as open-space filling, including within brecciated zones. Specifically, in this extensional context, low-angle detachment faulting led to the formation of open spaces between fragments of brecciated country rocks (e.g., serpentinite; Tourneur et al., 2021; figs. 2B, 2C). Consequently, euhedral to subhedral minerals (e.g., arsenides and calcite; figs. 2B-D) could fill large-scale pockets in open spaces within an extensional environment (Tourneur et al., 2021). This tectonic setting would favor hydrothermal fluid flow and mineralization resulting from the involvement of two originally immiscible fluids (inset in fig. 6; En-Naciri et al., 1997; Essarraj et al., 2005). Previous work on fluid inclusion data concluded that the first fluid was sodium-calcium chloride (NaCl-$CaCl_2$), seawater-derived brines (En-Naciri et al., 1997; Essarraj et al., 2005). These brines, which were saturated with respect to halite, had salinities (5.5 to 22.0 weight percent equivalent [wt.% eq.] NaCl and 13.5 to 18.5 wt.% eq. $CaCl_2$) two to six times the average Cambrian–Devonian seawater salinity (Demicco et al., 2005; En-Naciri et al., 1997; Essarraj et al., 2005). Fluid inclusion halogen and cation ratios are typical of deep basinal brines, in particular oil-field brines, which were derived from surface evaporation of seawater (Essarraj et al., 2005). Given the timing of Co-arsenide mineralization in the Upper Devonian, the $\delta^{18}O_{seawater}$ was likely at −0.10 ± 1.30‰ (Galili et al., 2019). Our new $\delta^{18}O_{fluid}$ and $\delta^{34}S_{skutterudite}$ data support previous observations and conclusions that primary seawa-

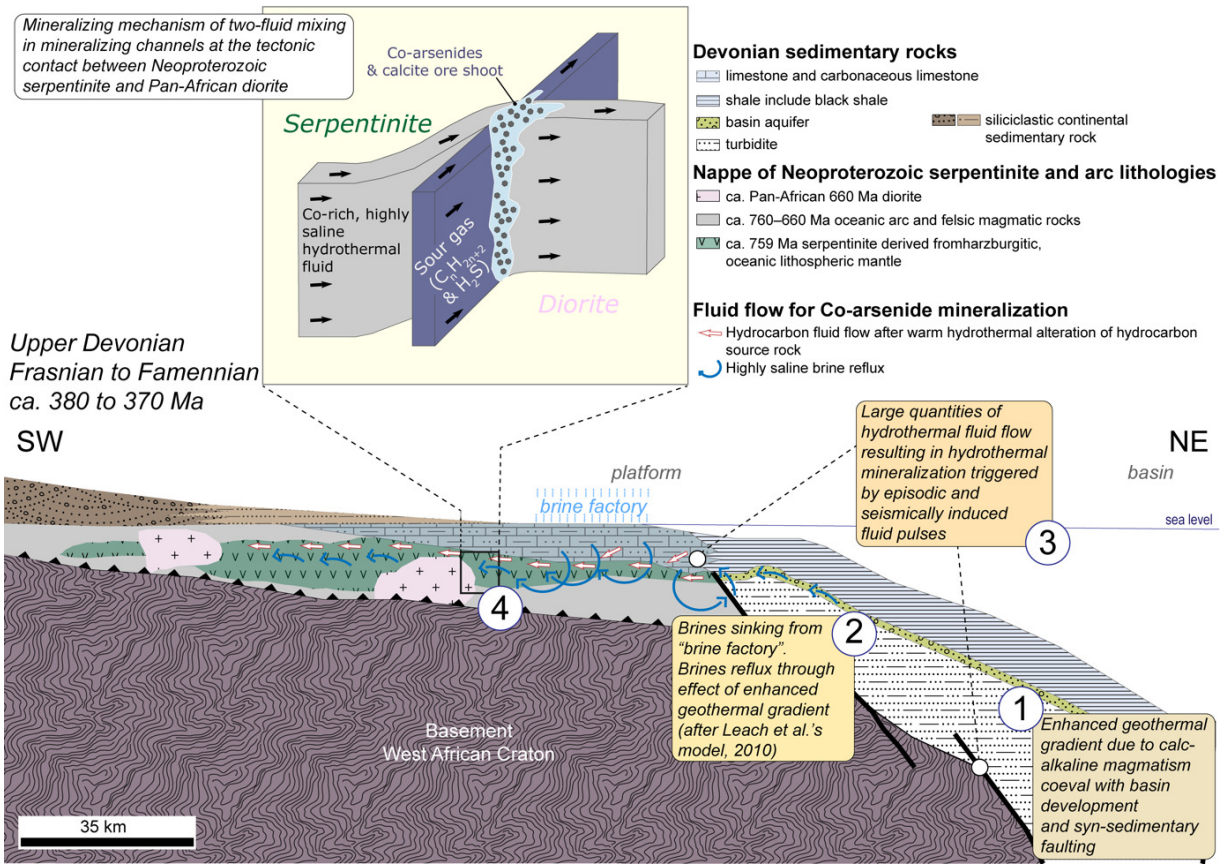

Figure 6. Proposed genetic model for Co-arsenide mineralization in the Upper Devonian between *ca.* 380 and 370 Ma at Bou Azzer

In the Upper Devonian, the central Anti-Atlas, including the Bou Azzer area, was a continental platform to major sedimentary basins located in the present-day eastern Anti-Atlas (Mader and Tafilalt Basins; fig. 1A). The sequentially numbered bullet points explain how the various items of this greater geodynamic context led to Co-arsenide mineralization at Bou Azzer. The inset shows our interpretation of the mineralizing processes leading to Co-arsenide mineralization in the geological context of the Aït Ahmane deposit in the Bou Azzer district. This inset figure of mineralization in ore shoots at the tectonic contacts between serpentinite and diorite is adapted from the general model for "five element-type mineralization" of Markl et al. (2016). See text for details.

ter-derived brines in the Bou Azzer region were modified by fluid-rock interaction during burial and migration through basement rocks: (1) The calculated $\delta^{18}O_{fluid}$ for Bou Azzer is a testament of limited fluid-rock interaction during burial and migration of the evaporative primary brines that evolved to the chemistry of deep basinal oil-field brines (En-Naciri et al., 1997; Essarraj et al., 2005), until eventual calcite precipitation in open spaces at the contact between serpentinite and diorite ($\delta^{18}O_{fluid}$ of −0.34 to +1.90‰) and calcite associated with Co-arsenides ($\delta^{18}O_{fluid}$ of +1.26 to +3.72‰). Assuming that the temperatures of calcite precipitation determined from clumped isotope data were not reset after the original arsenide-calcite mineralization, and considering that calcite follows arsenides in the paragenetic sequence (fig. 2A), the minimum temperatures of calcite precipitation (146–219 °C) are compatible with previous temperature estimates of Bou Azzer Co-arsenide mineralization at *ca.* 200 to 225 °C (En-Naciri et al., 1997; Essarraj et al., 2005); (2) Low Na/Ca ratios in fluid inclusions are diagnostic of the interaction of Na-rich brines with Ca-rich rocks because brines that evaporate beyond the point of halite saturation should have high Na/Ca ratios (Essarraj et al., 2005). At Bou Azzer, a gain in Ca is related to feldspar alteration in diorite (Ca-Na exchange during albitization of plagioclase; Essarraj et al., 2005; Leblanc & Lbouabi, 1988; fig. 2D) during brine migration at the interface with serpentinite (fig. 6). The sulfur isotope composition of skutterudite ($\delta^{34}S_{skutterudite}$ = +1.00 ± 0.18 to +4.91 ± 0.39‰) is compatible with derivation of hydrogen sulfide from trace magmatic sulfides in diorite during this hydrothermal alteration.

The seawater-derived brines coexisted with another fluid comprising methane ± molecular nitrogen ($CH_4 \pm N_2$) gas (En-Naciri et al., 1997; Essarraj et al., 2005). The ore-stage calcite $\delta^{13}C$ and $\delta^{18}O$ isotope data overlap with the $\delta^{13}C$ and $\delta^{18}O$ values of calcite in sediment-hosted petroleum reservoirs worldwide (e.g., Alberta, Canada; fig. 4A), and with replacement and pore-filling calcite veins associated with bitumen in basalt-hosted petroleum reservoirs in Greenland (Rogers et al., 2006). In such geological settings, $\delta^{13}C$ of calcite cements is diagnostic of the processes altering hydrocarbons in reservoirs (fig. 4B; Macaulay et al.,

2000). Thus, the $\delta^{13}C$ composition of calcite may commonly reflect a mixing of marine bicarbonate ($\delta^{13}C$ of *ca.* 0‰) with dissolved inorganic carbon with light $\delta^{13}C$ values (<−25‰) derived from altered organic matter (Peckmann et al., 1999). Here, we propose that calcite at Bou Azzer results from the interaction of basinal brines with CH_4–N_2 gaseous fluids, involving the abiotic degradation of hydrocarbons at the site of arsenide mineralization. The resulting pool of dissolved inorganic carbon available to form calcite with $\delta^{13}C$ values of −4.64 ± 0.04 to −3.92 ± 0.01‰ would be dominated by marine bicarbonate with only a minor contribution from methane decomposition (fig. 4B).

This methane gas was probably sour gas, 'i.e.', hydrocarbon gases bearing hydrogen sulfide (H_2S) with a light sulfur isotope composition (G. M. Anderson, 2008). This interpretation is supported by the isotopically light $\delta^{34}S$ values of $NiAs_2$ (−8.31 ± 0.18‰) and $CoAs_2$ (−7.63 ± 0.20 to −5.21 ± 0.10‰) at Bou Azzer (fig. 2D). Thermal decarboxylation of hydrocarbons (Macaulay et al., 2000) is a process of hydrocarbon degradation that is compatible with the $\delta^{13}C$ signatures of Bou Azzer calcite (fig. 4B; Irwin et al., 1977; Macaulay et al., 2000). This degradation of hydrocarbons is probably the pre-requisite for mixing of the two above-mentioned fluids that were initially immiscible. We conceptualize that the oxidation of organic molecules mainly controlled the reduction of As for arsenide mineralization (see details in the next section).

Considering the present new findings and consequent genetic model for Co-arsenide mineralization at Bou Azzer (fig. 6), the identification of the exact hydrocarbon source rocks should be the aim of future studies (see section 5 and the detailed explanations of limitation #2 about the present work). Yet, there are several working hypotheses regarding the source(s) of hydrocarbons on which we speculate here. In the context of extensional tectonics in the central and eastern Anti-Atlas in the Devonian, several sources of hydrocarbon accumulations (especially methane) are possible for explaining the sudden influx and availability of methane gas for arsenide mineralization (according to the model by Markl et al., 2016) in the Bou Azzer area. On the one hand, carbonate mounds related to methane ± H_2S venting in sedimentary basins in the Emsian and Eifelian–Givetian are known as the "Kess Kess" and "Hollard" Mounds in the eastern Anti-Atlas, respectively (fig. 1A; Belka et al., 2018; Peckmann et al., 1999). On the other hand, deposition of black bituminous limestone and shale took place in shallow basins (eastern Anti-Atlas) and adjacent pelagic platforms (including the Bou Azzer area in central Anti-Atlas; fig. 1A) during the Kellwasser event as summarized in the previous section (Wendt & Belka, 1991). The timing of this "Moroccan" Upper Kellwasser event (*ca.* 373 to 371 Ma) overlaps with or slightly precedes the time of extensive fine-grained Co-arsenide mineralization at Bou Azzer determined here (*ca.* 373.4 to 368.1 Ma), whereas the "Moroccan" Lower Kellwasser episode at *ca.* 382–381 Ma shortly precedes the timing of a first stage of coarse-grained safflorite mineralization at ca 380.4 Ma (fig. 5). Therefore, our geochronological and lithological evidence would collectively favor the hypothesis that supply and migration of hydrocarbons (including methane) from hydrocarbon source rocks in the Bou Azzer platform (fig. 6) probably took place following warm hydrothermal alteration of Upper Devonian Kellwasser hydrocarbon source rocks ('i.e.', either carbonaceous limestone or organic-rich shale) by heated, seawater-derived basinal brines. We cannot exclude that hydrocarbons (1) were also produced by warm hydrothermal alteration of Upper Devonian Kellwasser hydrocarbon source rocks deposited in the basins adjacent to the Bou Azzer platform, and (2) migrated from basin to platform setting. In fact, hydrocarbon migration from basin to carbonate platform is known in the petroleum systems related to Jurassic hydrocarbon sources rocks in the Gotnia and Arabian basins in south-western Iraq and Central Saudi Arabia. In such systems, hydrocarbon migration took place up dip and laterally in permeable conduits (Fox & Ahlbrandt, 2002).

4.3. Source of metals and reduction pathways for Co-arsenide mineralization

Osmium isotope data and microscopic observations reported here provide new insights into the source of metals and the chemical and mineralogical controls on the mechanisms of reduction leading to Co-arsenide mineralization at Bou Azzer. Serpentinites derived from Re-depleted, harzburgitic, oceanic lithospheric mantle possess unradiogenic $^{187}Os/^{188}Os$ ratios (Agranier et al., 2007; Meisel et al., 1996; Reisberg et al., 1991; Smith et al., 2021) that fall within the range of $^{187}Os/^{188}Os$ ratios reported for fresh lithospheric mantle harzburgite peridotite (0.118–0.128; Snow & Reisberg, 1995). Such Os isotopic signatures are explained by serpentinization at low fugacity of hydrogen sulfide that results in newly formed Os-rich alloys retaining the unradiogenic $^{187}Os/^{188}Os$ composition of primary mantle sulfides in the original unaltered peridotite (Foustoukos et al., 2015). The Os_i of safflorite at 0.120 ± 0.001 points to a derivation of Os from the pre-existing serpentinized oceanic lithosphere including harzburgite at Bou Azzer (Hodel et al., 2020) that was leached by highly saline basinal brines in the Late Devonian. By corollary, using Os a tracer for the source of other metals (Saintilan et al., 2021), serpentinite logically stands as a major source of cobalt and nickel (Bouabdellah et al., 2016; Leblanc & Billaud, 1982) that could be leached effectively by NaCl-$CaCl_2$-bearing basinal brines (Liu et al., 2011, 2012; Williams-Jones & Vasyukova, 2022). Such hydrothermal fluids have the chemistry to effectively leach and transport cobalt (Liu et al., 2012).

The hydrothermal alteration of pre-existing Neoproterozoic serpentinite by acidic, Cl-rich fluids in the Late Devonian led to the formation of distinctive massive magnetite veins within serpentinite at Bou Azzer (Hodel et al., 2017). This process resulted in an increase in modal magnetite content with veins of secondary magnetite augmenting the primary disseminated magnetite that formed during serpentinization in the Neoproterozoic (Hodel et al., 2017). These magnetite veins signal the availability and mobility of iron from serpentinite, probably in the form of aqueous Fe(II)-Cl_2 species (Debret et al., 2016). Therefore, by piec-

ing together evidence for the involvement of an oil-field brine system with the availability and mobility of reduced Fe(II), we conceptualize two pathways of reduction of arsenic leading to the production of reduced species of arsenic available for Co-Ni-arsenide mineralization:

1. an abiotic process of reduction of As(V) by Fe(II) as previously evidenced in sub-surface settings in studies dealing with environmental monitoring of groundwater quality (Bose & Sharma, 2002). Such a process taking place in deeper crustal settings at Bou Azzer would equally explain petrographic observations whereby magnetite in serpentinite is replaced by Ni-arsenides in particular (Tourneur et al., 2021); and
2. an additional pathway involving the abiotic thermal decarboxylation of hydrocarbon mentioned above. The oxidation of hydrocarbons would be accompanied by reduction of arsenic species and a decrease in solubility of aqueous Co-chloride and Ni-chloride species that would dissociate to form cobalt and nickel arsenides (see Markl et al., 2016). The newly produced dissolved inorganic carbon derived from the oxidation of hydrocarbon would be fixed in calcite in breccia zone within serpentinite, and at the rheological contact between serpentinite and diorite (figs. 2B, 2C).

5. LIMITATIONS AND OPEN QUESTIONS

Limitation #1. Although serpentinites are known to be sponges for As (Deschamps et al., 2010; Hattori et al., 2005; Ryan et al., 2011), a demonstration that the Bou Azzer serpentinite is not only the source of Co and Ni but also a volumetrically sufficient local source of As remains necessary ('i.e.', through replacement of As-bearing magnetite by arsenides and leaching of As at a specific oxidation state from the lattice of serpentine minerals; Hattori et al., 2005; Wu et al., 2021). Such a study would probably signal that a prerequisite for the formation of giant Co-Ni-arsenide ore deposits versus the numerous Co-Ni arsenide mineral occurrences in basement rocks of supercontinents (see Burisch et al., 2022) is the presence of serpentinite that acts as a source of both metals and metalloid (As).

Limitation #2. Our present study calls for follow-up work that could yield direct geochemical evidence in support of our preferred hypothesis that hydrocarbons involved in mineralization at Bou Azzer were sourced from shale hydrocarbon source rocks and/or dark bituminous fetid limestone deposited at the time of the Kellwasser biotic crisis. We suggest that compound-specific carbon isotope data combined with organic geochemical studies of a suite of samples comprising arsenides, calcite, serpentinite, and Kellwasser source rocks may prove fruitful.

Acknowledgments

N.J.S., M.I. and M.S. are indebted to the administration and employees of the CTT-Managem Group at Bou Azzer for their kind hospitality and logistical support during fieldwork. N.J.S. acknowledges support from the Swiss National Science Foundation through an Ambizione Fellowship (Grant PZ00P2_180133). M.I. acknowledges financial support from Ibn Zohr University, Agadir, Morocco. R.A.C. acknowledges an NSERC Discovery Grant. Dr. J. Slack (Emeritus USGS) is thanked for his constructive comments on an earlier version of this manuscript. We thank Associate Editor Ethan Baxter and reviewer Alan D. Rooney for stimulating, constructive, and pertinent comments and thoughtful advice to clarify several points in our manuscript. The additional comments by an anonymous reviewer are acknowledged. The overall editorial handling by Editor-in-chief Page Chamberlain is greatly appreciated as well as additional constructive comments throughout the review process.

Author contributions

N.J.S. and M.I. designed the study. N.J.S., M.I., M.S. performed fieldwork and sample collection. A.K. and L.M. organized fieldwork and contributed to sample collection. N.J.S. carried out petrographic investigations, mineral separation, arsenide Re-Os isotope geochemistry procedures and N-TIMS mass spectrometry analyzes at ETH Zürich. J.T. and R.A.C. conducted arsenide Re-Os isotope geochemistry procedures and N-TIMS mass spectrometry analyzes at the University of Alberta on aliquots provided by N.J.S. S.M.B. performed carbon, oxygen and clumped isotope analyzes of calcite using samples prepared by N.J.S. J.E.S. performed sulfur stable isotope analyzes of arsenides using samples prepared by N.J.S. N.J.S. and J.M.A. performed mineral chemistry analyzes. N.J.S. wrote the paper. All co-authors contributed comments and improvements to both the original draft and the revised manuscript.

Data and materials availability

All data are available in the main text or the supplementary materials.

Supplementary Data

https://earth.eps.yale.edu/~ajs/SupplementaryData/2023/Saintilan/"

Editor: C. Page Chamberlain, Associate Editor: Ethan Baxter

Submitted: February 07, 2023 EDT. Accepted: December 02, 2023 EDT. Published: December 31, 2023 EDT.

REFERENCES

Agranier, A., Lee, C.-T. A., Li, Z.-X. A., & Leeman, W. P. (2007). Fluid-mobile element budgets in serpentinized oceanic lithospheric mantle: Insights from B, As, Li, Pb, PGEs and Os isotopes in the Feather River Ophiolite, California. *Chemical Geology*, *245*(3–4), 230–241. https://doi.org/10.1016/j.chemgeo.2007.08.008

Ahmed, A. H., Arai, S., & Ikenne, M. (2009). Mineralogy and Paragenesis of the Co-Ni Arsenide Ores of Bou Azzer, Anti-Atlas, Morocco. *Economic Geology*, *104*(2), 249–266. https://doi.org/10.2113/gsecongeo.104.2.249

Allaz, J. M., Williams, M. L., Jercinovic, M. J., Goemann, K., & Donovan, J. (2019). Multipoint Background Analysis: Gaining Precision and Accuracy in Microprobe Trace Element Analysis. *Microscopy and Microanalysis*, *25*(1), 30–46. https://doi.org/10.1017/s1431927618015660

Anderson, G. M. (2008). The mixing hypothesis and the origin of Mississippi Valley-type ore deposits. *Economic Geology*, *103*(8), 1683–1690. https://doi.org/10.2113/gsecongeo.103.8.1683

Anderson, N. T., Kelson, J. R., Kele, S., Daëron, M., Bonifacie, M., Horita, J., Mackey, T. J., John, C. M., Kluge, T., Petschnig, P., Jost, A. B., Huntington, K. W., Bernasconi, S. M., & Bergmann, K. D. (2021). A Unified Clumped Isotope Thermometer Calibration (0.5–1,100°C) Using Carbonate-Based Standardization. *Geophysical Research Letters*, *48*(7). https://doi.org/10.1029/2020gl092069

Armstrong, J. T. (1988). Quantitative analysis of silicate and oxide minerals: comparison of Monte Carlo, ZAF and phi-rho-z procedures. *Analysis Microbeam*, 239–246.

Belka, Z., Skompski, S., Dopieralska, J., & Feist, R. (2018). Flow paths of hydrothermal vent fluids in the Devonian Kess-Kess mounds, Anti-Atlas, Morocco. *Neues Jahrbuch für Geologie und Paläontologie - Abhandlungen*, *290*(1–3), 49–63. https://doi.org/10.1127/njgpa/2018/0779

Bernasconi, S. M., Daëron, M., Bergmann, K. D., Bonifacie, M., Meckler, A. N., Affek, H. P., Anderson, N., Bajnai, D., Barkan, E., Beverly, E., Blamart, D., Burgener, L., Calmels, D., Chaduteau, C., Clog, M., Davidheiser-Kroll, B., Davies, A., Dux, F., Eiler, J., ... Ziegler, M. (2021). InterCarb: A community effort to improve interlaboratory standardization of the carbonate clumped isotope thermometer using carbonate standards. *Geochemistry, Geophysics, Geosystems*, *22*(5), e2020GC009588. https://doi.org/10.1029/2020gc009588

Birck, J. L., Barman, M. R., & Capmas, F. (1997). Re-Os Isotopic Measurements at the Femtomole Level in Natural Samples. *Geostandards Newsletter*, *21*(1), 19–27. https://doi.org/10.1111/j.1751-908x.1997.tb00528.x

Bose, P., & Sharma, A. (2002). Role of iron in controlling speciation and mobilization of arsenic in subsurface environment. *Water Research*, *36*(19), 4916–4926. https://doi.org/10.1016/s0043-1354(02)00203-8

Bouabdellah, M., Maacha, L., Levresse, G., & Saddiqi, O. (2016). The Bou Azzer Co-Ni-Fe-As(±Au ± Ag) District of Central Anti-Atlas (Morocco): A Long-Lived Late Hercynian to Triassic Magmatic-Hydrothermal to Low-Sulphidation Epithermal System. In M. Bouabdellah & J. F. Slack (Eds.), *Mineral Deposits of North Africa, Mineral Resource Reviews* (pp. 229–247). Springer. https://doi.org/10.1007/978-3-319-31733-5_8

Bozhkov, O. D., Jordanov, N., Borissova, L. V., & Fabelinskii, Y. I. (1985). Extraction-spectral emission determination of traces of rhenium using ICP. *Fresenius' Zeitschrift für analytische Chemie*, *321*(5), 453–456. https://doi.org/10.1007/bf00487078

Brenan, J. M., Cherniak, D. J., & Rose, L. A. (2000). Diffusion of osmium in pyrrhotite and pyrite: implications for closure of the Re–Os isotopic system. *Earth and Planetary Science Letters*, *180*(3–4), 399–413. https://doi.org/10.1016/s0012-821x(00)00165-5

Burisch, M., Markl, G., & Gutzmer, J. (2022). Breakup with benefits - hydrothermal mineral systems related to the disintegration of a supercontinent. *Earth and Planetary Science Letters*, *580*, 117373. https://doi.org/10.1016/j.epsl.2022.117373

Carmichael, S. K., Waters, J. A., Königshof, P., Suttner, T. J., & Kido, E. (2019). Paleogeography and paleoenvironments of the Late Devonian Kellwasser event: A review of its sedimentological and geochemical expression. *Global and Planetary Change*, *183*, 102984. https://doi.org/10.1016/j.gloplacha.2019.102984

Chantler, C. T., Olsen, K., Dragoset, R. A., Chang, J., Kishore, A. R., Kotochigova, S. A., & Zucker, D. S. (2005). *X-Ray Form Factor, Attenuation and Scattering Tables* (version 2.1). National Institute of Standards and Technology. http://physics.nist.gov/ffast

Chiaradia, M., Schaltegger, U., Spikings, R., Wotzlaw, J.-F., & Ovtcharova, M. (2013). How Accurately Can We Date the Duration of Magmatic-Hydrothermal Events in Porphyry Systems?--An Invited Paper. *Economic Geology*, *108*(4), 565–584. https://doi.org/10.2113/econgeo.108.4.565

Cohen, A. S., & Waters, F. G. (1996). Separation of osmium from geological materials by solvent extraction for analysis by thermal ionisation mass spectrometry. *Analytica Chimica Acta*, *332*(2–3), 269–275. https://doi.org/10.1016/0003-2670(96)00226-7

Creaser, R. A., Papanastassiou, D. A., & Wasserburg, G. J. (1991). Negative thermal ion mass spectrometry of osmium, rhenium and iridium. *Geochimica et Cosmochimica Acta*, *55*(1), 397–401. https://doi.org/10.1016/0016-7037(91)90427-7

Cumming, V. M., Poulton, S. W., Rooney, A. D., & Selby, D. (2013). Anoxia in the terrestrial environment during the late Mesoproterozoic. *Geology*, *41*(5), 583–586. https://doi.org/10.1130/g34299.1

Daëron, M., Blamart, D., Peral, M., & Affek, H. P. (2016). Absolute isotopic abundance ratios and the accuracy of Δ47 measurements. *Chemical Geology*, *442*, 83–96. https://doi.org/10.1016/j.chemgeo.2016.08.014

Davies, T., Richards, J. P., Creaser, R. A., Heaman, L. M., Chacko, T., Simonetti, A., Williamson, J., & McDonald, D. W. (2010). Paleoproterozoic Age Relationships in the Three Bluffs Archean Iron Formation-Hosted Gold Deposit, Committee Bay Greenstone Belt, Nunavut, Canada. *Exploration and Mining Geology*, *19*(3–4), 55–80. https://doi.org/10.2113/gsemg.19.3-4.55

De Vleeschouwer, D., Da Silva, A.-C., Sinnesael, M., Chen, D., Day, J. E., Whalen, M. T., Guo, Z., & Claeys, P. (2017). Timing and pacing of the Late Devonian mass extinction event regulated by eccentricity and obliquity. *Nature Communications*, *8*(1). https://doi.org/10.1038/s41467-017-02407-1

Debret, B., Millet, M.-A., Pons, M.-L., Bouilhol, P., Inglis, E., & Williams, H. (2016). Isotopic evidence for iron mobility during subduction. *Geology*, *44*(3), 215–218. https://doi.org/10.1130/g37565.1

Demicco, R. V., Lowenstein, T. K., Hardie, L. A., & Spencer, R. J. (2005). Model of seawater composition for the Phanerozoic. *Geology*, *33*(11), 877–880. https://doi.org/10.1130/g21945.1

Deschamps, F., Guillot, S., Godard, M., Chauvel, C., Andreani, M., & Hattori, K. (2010). In situ characterization of serpentinites from forearc mantle wedges: Timing of serpentinization and behavior of fluid-mobile elements in subduction zones. *Chemical Geology*, *269*(3–4), 262–277. https://doi.org/10.1016/j.chemgeo.2009.10.002

Devleeschouwer, X., Herbosch, A., & Préat, A. (2002). Microfacies, sequence stratigraphy and clay mineralogy of a condensed deep-water section around the Frasnian/Famennian boundary (Steinbruch Schmidt, Germany). *Palaeogeography, Palaeoclimatology, Palaeoecology*, *181*(1–3), 171–193. https://doi.org/10.1016/s0031-0182(01)00478-3

En-Naciri, A., Barbanson, L., & Touray, J.-C. (1997). Brine inclusions from the Co-As(Au) Bou Azzer District, Anti-Atlas Mountains, Morocco. *Economic Geology*, *92*(3), 360–367. https://doi.org/10.2113/gsecongeo.92.3.360

Essarraj, S., Boiron, M.-C., Cathelineau, M., Banks, D. A., & Benharref, M. (2005). Penetration of surface-evaporated brines into the Proterozoic basement and deposition of Co and Ag at Bou Azzer (Morocco): Evidence from fluid inclusions. *Journal of African Earth Sciences*, *41*(1–2), 25–39. https://doi.org/10.1016/j.jafrearsci.2005.03.001

Ez-Zghoudy, M., Ikenne, M., Souhassou, M., Belfoul, M. A., Gouiza, M., Ilmen, S., Ousbih, M., Karfal, A., Maacha, L., & Zouhair, M. (2023). Structural controls on the Co and Ni-bearing arsenides from the Bou Azzer mine (Case of Aït Ahmane F53 vein deposit): Implications for mineral exploration. *Journal of African Earth Sciences*, *202*, 104929. https://doi.org/10.1016/j.jafrearsci.2023.104929

Foustoukos, D. I., Bizimis, M., Frisby, C., & Shirey, S. B. (2015). Redox controls on Ni–Fe–PGE mineralization and Re/Os fractionation during serpentinization of abyssal peridotite. *Geochimica et Cosmochimica Acta*, *150*, 11–25. https://doi.org/10.1016/j.gca.2014.11.025

Fox, J. E., & Ahlbrandt, T. S. (2002). Petroleum geology and total petroleum systems of the Widyan Basin and interior platform of Saudi Arabia and Iraq. *US Geological Survey Bulletin*, *2202-E*.

Franchi, F., Cavalazzi, B., Pierre, C., & Barbieri, R. (2015). New evidences of hydrothermal fluids circulation at the Devonian Kess Kess mounds, Hamar Laghdad (eastern Anti-Atlas, Morocco). *Geological Journal*, *50*(5), 634–650. https://doi.org/10.1002/gj.2582

Frizon de Lamotte, D., Tavakoli-Shirazi, S., Leturmy, P., Averbuch, O., Mouchot, N., Raulin, C., Leparmentier, F., Blanpied, C., & Ringenbach, J.-C. (2013). Evidence for Late Devonian vertical movements and extensional deformation in northern Africa and Arabia: Integration in the geodynamics of the Devonian world. *Tectonics*, *32*(2), 107–122. https://doi.org/10.1002/tect.20007

Galili, N., Shemesh, A., Yam, R., Brailovsky, I., Sela-Adler, M., Schuster, E. M., Collom, C., Bekker, A., Planavsky, N., Macdonald, F. A., Préat, A., Rudmin, M., Trela, W., Sturesson, U., Heikoop, J. M., Aurell, M., Ramajo, J., & Halevy, I. (2019). The geologic history of seawater oxygen isotopes from marine iron oxides. *Science*, *365*(6452), 469–473. https://doi.org/10.1126/science.aaw9247

Gasquet, D., Levresse, G., Cheilletz, A., Azizi-Samir, M. R., & Mouttaqi, A. (2005). Contribution to a geodynamic reconstruction of the Anti-Atlas (Morocco) during Pan-African times with the emphasis on inversion tectonics and metallogenic activity at the Precambrian–Cambrian transition. *Precambrian Research*, *140*(3–4), 157–182. https://doi.org/10.1016/j.precamres.2005.06.009

Gramlich, J. W., Murphy, T. J., Garner, E. L., & Shields, W. R. (1973). Absolute isotopic abundance ratio and atomic weight of a reference sample of rhenium. *Journal of Research of the National Bureau of Standards Section A: Physics and Chemistry*, *77A*(6), 691–698. https://doi.org/10.6028/jres.077a.040

Hattori, K., Takahashi, Y., Guillot, S., & Johanson, B. (2005). Occurrence of arsenic (V) in forearc mantle serpentinites based on X-ray absorption spectroscopy study. *Geochimica et Cosmochimica Acta*, *69*(23), 5585–5596. https://doi.org/10.1016/j.gca.2005.07.009

Hnatyshin, D., Kontak, D. J., Turner, E. C., Creaser, R. A., Morden, R., & Stern, R. A. (2016). Geochronologic (Re Os) and fluid-chemical constraints on the formation of the Mesoproterozoic-hosted Nanisivik Zn Pb deposit, Nunavut, Canada: Evidence for early diagenetic, low-temperature conditions of formation. *Ore Geology Reviews*, *79*, 189–217. https://doi.org/10.1016/j.oregeorev.2016.05.017

Hodel, F., Macouin, M., Triantafyllou, A., Carlut, J., Berger, J., Rousse, S., Ennih, N., & Trindade, R. I. F. (2017). Unusual massive magnetite veins and highly altered Cr-spinels as relics of a Cl-rich acidic hydrothermal event in Neoproterozoic serpentinites (Bou Azzer ophiolite, Anti-Atlas, Morocco). *Precambrian Research*, *300*, 151–167. https://doi.org/10.1016/j.precamres.2017.08.005

Hodel, F., Triantafyllou, A., Berger, J., Macouin, M., Baele, J.-M., Mattielli, N., Monnier, C., Trindade, R. I. F., Ducea, M. N., Chatir, A., Ennih, N., Langlade, J., & Poujol, M. (2020). The Moroccan Anti-Atlas ophiolites: Timing and melting processes in an intra-oceanic arc-back-arc environment. *Gondwana Research*, *86*, 182–202. https://doi.org/10.1016/j.gr.2020.05.014

Hollard, H. (1974). Recherches sur la stratigraphie des formations du Dévonien moyen, de l'Emsien supérieur au Frasnien, dans le Sud du Tafilait et dans le Ma'der (Anti-Atlas oriential). *Notes et Mémoires du Service Géologique du Maroc*, *264*, 7–68.

Horn, S., Gunn, A. G., Petavratzi, E., Shaw, R. A., Eilu, P., Törmänen, T., Bjerkgård, T., Sandstad, J. S., Jonsson, E., Kountourelis, S., & Wall, F. (2021). Cobalt resources in Europe and the potential for new discoveries. *Ore Geology Reviews*, *130*, 103915. https://doi.org/10.1016/j.oregeorev.2020.103915

Ikenne, M., Souhassou, M., Saintilan, N. J., Karfal, A., Hassani, A. E. L., Moundi, Y., Ousbih, M., Ezzghoudi, M., Zouhir, M., & Maacha, L. (2021). Cobalt–nickel–copper arsenide, sulfarsenide and sulfide mineralization in the Bou Azzer window, Anti-Atlas, Morocco: one century of multi-disciplinary and geological investigations, mineral exploration and mining. *Geological Society, London, Special Publications*, *502*(1), 45–66. https://doi.org/10.1144/sp502-2019-132

Irwin, H., Curtis, C., & Coleman, M. (1977). Isotopic evidence for source of diagenetic carbonates formed during burial of organic-rich sediments. *Nature*, *269*(5625), 209–213. https://doi.org/10.1038/269209a0

John, C. M., & Bowen, D. (2016). Community software for challenging isotope analysis: First applications of 'Easotope' to clumped isotopes. *Rapid Communications in Mass Spectrometry*, *30*(21), 2285–2300. https://doi.org/10.1002/rcm.7720

Johnson, J. P., & Cross, K. C. (1995). U-Pb geochronological constraints on the genesis of the Olympic Dam Cu-U-Au-Ag deposit, South Australia. *Economic Geology*, *90*(5), 1046–1063. https://doi.org/10.2113/gsecongeo.90.5.1046

Leach, D. L., Bradley, D. C., Huston, D., Pisarevsky, S. A., Taylor, R. D., & Gardoll, S. J. (2010). Sediment-Hosted Lead-Zinc Deposits in Earth History. *Economic Geology*, *105*(3), 593–625. https://doi.org/10.2113/gsecongeo.105.3.593

Leblanc, M. (1981). Chapter 17 The Late Proterozoic Ophiolites of Bou Azzer (Morocco): Evidence for Pan-African Plate Tectonics. *Developments in Precambrian Geology*, *4*, 435–451. https://doi.org/10.1016/s0166-2635(08)70022-7

Leblanc, M., & Billaud, P. (1982). Cobalt arsenide orebodies related to an upper Proterozoic ophiolite; Bou Azzer (Morocco). *Economic Geology*, *77*(1), 162–175. https://doi.org/10.2113/gsecongeo.77.1.162

Leblanc, M., & Lbouabi, M. (1988). Native silver mineralization along a rodingite tectonic contact between serpentinite and quartz diorite (Bou Azzer, Morocco). *Economic Geology*, *83*(7), 1379–1391. https://doi.org/10.2113/gsecongeo.83.7.1379

Levresse, G. (2001). *Contribution à l'établissement d'un modèle génétique des gisements d'Imiter (As-Hg), Bou Madine (Pb-Zn-Ag-Au) et Bou Azzer (Co-Ni-As-Au-Ag) dans l'Anti-Atlas marocain* [PhD Thesis]. INPL.

Li, C., Qu, W., Du, A., & Sun, W. (2009). Comprehensive study on extraction of rhenium with acetone in Re-Os isotopic dating. *Rock and Mineral Analysis*, *28*, 233–238.

Li, Y., Selby, D., Condon, D., & Tapster, S. (2017). Cyclic Magmatic-Hydrothermal Evolution in Porphyry Systems: High-Precision U-Pb and Re-Os Geochronology Constraints on the Tibetan Qulong Porphyry Cu-Mo Deposit. *Economic Geology*, *112*(6), 1419–1440. https://doi.org/10.5382/econgeo.2017.4515

Li, Y., & Vermeesch, P. (2021). Short communication: Inverse isochron regression for Re–Os, K–Ca and other chronometers. *Geochronology*, *3*(2), 415–420. https://doi.org/10.5194/gchron-3-415-2021

Liu, W., Borg, S. J., Testemale, D., Etschmann, B., Hazemann, J.-L., & Brugger, J. (2011). Speciation and thermodynamic properties for cobalt chloride complexes in hydrothermal fluids at 35–440°C and 600bar: An in-situ XAS study. *Geochimica et Cosmochimica Acta*, *75*(5), 1227–1248. https://doi.org/10.1016/j.gca.2010.12.002

Liu, W., Migdisov, A., & Williams-Jones, A. (2012). The stability of aqueous nickel(II) chloride complexes in hydrothermal solutions: Results of UV–Visible spectroscopic experiments. *Geochimica et Cosmochimica Acta*, *94*, 276–290. https://doi.org/10.1016/j.gca.2012.04.055

Ludwig, K. R. (1980). Calculation of uncertainties of U-Pb isotope data. *Earth and Planetary Science Letters*, *46*(2), 212–220. https://doi.org/10.1016/0012-821x(80)90007-2

Macaulay, C. I., Fallick, A. E., Haszeldine, R. S., & McAulay, G. E. (2000). Oil migration makes the difference: regional distribution of carbonate cement $\delta^{13}C$ in northern North Sea Tertiary sandstones. *Clay Minerals*, *35*(1), 69–76. https://doi.org/10.1180/000985500546738

Macmillan, E., Cook, N. J., Ehrig, K., & Pring, A. (2017). Chemical and textural interpretation of late-stage coffinite and brannerite from the Olympic Dam IOCG-Ag-U deposit. *Mineralogical Magazine*, *81*(6), 1323–1366. https://doi.org/10.1180/minmag.2017.081.006

Majzlan, J., Mikuš, T., Kiefer, S., & Creaser, R. A. (2022). Rhenium-osmium geochronology of gersdorffite and skutterudite-pararammelsbergite links nickel–cobalt mineralization to the opening of the incipient Meliata Ocean (Western Carpathians, Slovakia). *Mineralium Deposita*, *57*(4), 621–629. https://doi.org/10.1007/s00126-022-01101-7

Markey, R., Stein, H. J., Hannah, J. L., Zimmerman, A., Selby, D., & Creaser, R. A. (2007). Standardizing Re–Os geochronology: A new molybdenite Reference Material (Henderson, USA) and the stoichiometry of Os salts. *Chemical Geology*, *244*(1–2), 74–87. https://doi.org/10.1016/j.chemgeo.2007.06.002

Markl, G., Burisch, M., & Neumann, U. (2016). Natural fracking and the genesis of five-element veins. *Mineralium Deposita*, *51*(6), 703–712. https://doi.org/10.1007/s00126-016-0662-z

Matthews, A. D., & Riley, J. P. (1970). The determination of Rhenium in sea water. *Analytica Chimica Acta*, *51*(3), 483–488. https://doi.org/10.1016/s0003-2670(01)95744-7

Meckler, A. N., Ziegler, M., Millán, M. I., Breitenbach, S. F. M., & Bernasconi, S. M. (2014). Long-term performance of the Kiel carbonate device with a new correction scheme for clumped isotope measurements. *Rapid Communications in Mass Spectrometry*, *28*(15), 1705–1715. https://doi.org/10.1002/rcm.6949

Meisel, T., Walker, R. J., & Morgan, J. W. (1996). The osmium isotopic composition of the Earth's primitive upper mantle. *Nature*, *383*(6600), 517–520. https://doi.org/10.1038/383517a0

Morelli, R. M., Bell, C. C., Creaser, R. A., & Simonetti, A. (2010). Constraints on the genesis of gold mineralization at the Homestake Gold Deposit, Black Hills, South Dakota from rhenium–osmium sulfide geochronology. *Mineralium Deposita*, *45*(5), 461–480. https://doi.org/10.1007/s00126-010-0284-9

Morgan, J. W., Golightly, D. W., & Dorrzapf, A. F. (1991). Methods for the separation of rhenium, osmium and molybdenum applicable to isotope geochemistry. *Talanta*, *38*(3), 259–265. https://doi.org/10.1016/0039-9140(91)80045-2

Müller, I. A., Fernandez, A., Radke, J., van Dijk, J., Bowen, D., Schwieters, J., & Bernasconi, S. M. (2017). Carbonate clumped isotope analyses with the long-integration dual-inlet (LIDI) workflow: scratching at the lower sample weight boundaries. *Rapid Communications in Mass Spectrometry*, *31*(12), 1057–1066. https://doi.org/10.1002/rcm.7878

Nowell, G. M., Pearson, D. G., Parman, S. W., Luguet, A., & Hanski, E. (2008). Precise and accurate 186Os/188Os and 187Os/188Os measurements by Multi-collector Plasma Ionisation Mass Spectrometry, part II: Laser ablation and its application to single-grain Pt–Os and Re–Os geochronology. *Chemical Geology*, *248*(3–4), 394–426. https://doi.org/10.1016/j.chemgeo.2007.12.004

Oberthür, T., Melcher, F., Henjes-Kunst, F., Gerdes, A., Stein, H. J., Zimmerman, A., & El Ghorfi, M. (2009). Hercynian age of the cobalt-nickel arsenide (gold) ores, Bou Azzer, Anti-Atlas, Morocco: Re-Os, Sm-Nd, and U-Pb age determinations. *Economic Geology*, *104*(7), 1065–1079. https://doi.org/10.2113/econgeo.104.7.1065

O'Neil, J. R., Clayton, R. N., & Mayeda, T. K. (1969). Oxygen Isotope Fractionation in Divalent Metal Carbonates. *The Journal of Chemical Physics*, *51*(12), 5547–5558. https://doi.org/10.1063/1.1671982

Peckmann, J., Walliser, O. H., Riegel, W., & Reitner, J. (1999). Signatures of hydrocarbon venting in a Middle Devonian Carbonate Mound (Hollard Mound) at the Hamar Laghdad (Antiatlas, Morocco). *Facies*, *40*(1), 281–296. https://doi.org/10.1007/bf02537477

Percival, L. M. E., Davies, J. H. F. L., Schaltegger, U., De Vleeschouwer, D., Da Silva, A.-C., & Föllmi, K. B. (2018). Precisely dating the Frasnian–Famennian boundary: implications for the cause of the Late Devonian mass extinction. *Scientific Reports*, *8*(1), 9578. https://doi.org/10.1038/s41598-018-27847-7

Petavratzi, E., Gunn, G., & Kresse, C. (2019). *BCG Commodity review: Cobalt*. British Geological Survey Open-File Report. https://nora.nerc.ac.uk/id/eprint/534461/1/BGS_Commodity_Review_Cobalt.pdf

Pouclet, A., El Hadi, H., Bardintzeff, J.-M., Benharref, M., & Fekkak, A. (2017). Devonian to Early Carboniferous magmatic alkaline activity in the Tafilalt Province, Eastearn Morocco: An Eovariscan episode in the Gondwana margin, north of the West African Craton. *Journal of African Earth Sciences*, *129*, 814–841. https://doi.org/10.1016/j.jafrearsci.2017.01.030

Reisberg, L. C., Allègre, C. J., & Luck, J.-M. (1991). The Re Os systematics of the Ronda Ultramafic Complex of southern Spain. *Earth and Planetary Science Letters*, *105*(1–3), 196–213. https://doi.org/10.1016/0012-821x(91)90131-z

Rogers, K. L., Neuhoff, P. S., Pedersen, A. K., & Bird, D. K. (2006). CO2 metasomatism in a basalt-hosted petroleum reservoir, Nuussuaq, West Greenland. *Lithos*, *92*(1–2), 55–82. https://doi.org/10.1016/j.lithos.2006.04.002

Rooney, A. D., Hnatyshin, D., Toma, J., Saintilan, N. J., Millikin, A. E. G., Selby, D., & Creaser, R. A. (in press). Application of the 187Re-187Os geochronometer to crustal materials: systematics, methodology, data reporting and interpretation. *Geological Society of America Bulletin*.

Roy-Barman, M., & Allègre, C. J. (1995). 187Os/186Os in oceanic island basalts: tracing oceanic crust recycling in the mantle. *Earth and Planetary Science Letters*, *129*(1–4), 145–161. https://doi.org/10.1016/0012-821x(94)00238-t

Ryan, P. C., Kim, J., Wall, A. J., Moen, J. C., Corenthal, L. G., Chow, D. R., Sullivan, C. M., & Bright, K. S. (2011). Ultramafic-derived arsenic in a fractured bedrock aquifer. *Applied Geochemistry*, *26*(4), 444–457. https://doi.org/10.1016/j.apgeochem.2011.01.004

Saintilan, N. J., Archer, C., Maden, C., Samankassou, E., Bernasconi, S. M., Szumigala, D., Mahaffey, Z., West, A., & Spangenberg, J. E. (2023). Metal-rich organic matter and hot continental passive margin: drivers for Devonian copper-cobalt-germanium mineralization in dolomitized reef-bearing carbonate platform. *Mineralium Deposita*, *58*(1), 37–49. https://doi.org/10.1007/s00126-022-01123-1

Saintilan, N. J., Creaser, R. A., & Bookstrom, A. A. (2017). Re-Os systematics and geochemistry of cobaltite (CoAsS) in the Idaho cobalt belt, Belt-Purcell Basin, USA: Evidence for middle Mesoproterozoic sediment-hosted Co-Cu sulfide mineralization with Grenvillian and Cretaceous remobilization. *Ore Geology Reviews*, *86*, 509–525. https://doi.org/10.1016/j.oregeorev.2017.02.032

Saintilan, N. J., Creaser, R. A., Spry, P. G., & Hnatyshin, D. (2017). Re-Os Systematics of Löllingite and Arsenopyrite In Granulite-Facies Garnet Rocks: Insights Into the Metamorphic History and Thermal Evolution of the Broken Hill Block During the Early Mesoproterozoic (New South Wales, Australia). *The Canadian Mineralogist*, *55*(1), 29–44. https://doi.org/10.3749/canmin.1600039

Saintilan, N. J., Selby, D., Hughes, J. W., Schlatter, D., Kolb, J., & Boyce, A. (2020a). Mineral separation protocol for accurate and precise rhenium-osmium (Re-Os) geochronology and sulphur isotope composition of individual sulphide species. *MethodsX*, *7*, 100944. https://doi.org/10.1016/j.mex.2020.100944

Saintilan, N. J., Selby, D., Hughes, J. W., Schlatter, D. M., Kolb, J., & Boyce, A. (2020b). Source of gold in Neoarchean orogenic-type deposits in the North Atlantic Craton, Greenland: Insights for a proto-source of gold in sub-seafloor hydrothermal arsenopyrite in the Mesoarchean. *Precambrian Research*, *343*, 105717. https://doi.org/10.1016/j.precamres.2020.105717

Saintilan, N. J., Spangenberg, J. E., Chiaradia, M., Chelle-Michou, C., Stephens, M. B., & Fontboté, L. (2019). Petroleum as source and carrier of metals in epigenetic sediment-hosted mineralization. *Scientific Reports*, *9*(1), 8283. https://doi.org/10.1038/s41598-019-44770-7

Saintilan, N. J., Sproson, A. D., Selby, D., Rottier, B., Casanova, V., Creaser, R. A., Kouzmanov, K., Fontboté, L., Piecha, M., Gereke, M., & Zambito, J. J., IV. (2021). Osmium isotopic constraints on sulphide formation in the epithermal environment of magmatic-hydrothermal mineral deposits. *Chemical Geology*, *564*, 120053. https://doi.org/10.1016/j.chemgeo.2020.120053

Scherstén, A., Szilas, K., Creaser, R. A., Næraa, T., van Gool, J. A. M., & Østergaard, C. (2012). Re–Os and U–Pb constraints on gold mineralisation events in the Meso- to Neoarchaean Storø greenstone belt, Storø, southern West Greenland. *Precambrian Research*, *200–203*, 149–162. https://doi.org/10.1016/j.precamres.2011.12.014

Schindler, I. (1990). *Die Kellwasser-Krise (hohe Frasne-Stufe, Ober-Devon)* [Doctoral dissertation]. Göttingen Göttinger Arbeite Geologische Paläontologie.

Schmid, T. W., & Bernasconi, S. M. (2010). An automated method for 'clumped-isotope' measurements on small carbonate samples. *Rapid Communications in Mass Spectrometry*, *24*(14), 1955–1963. https://doi.org/10.1002/rcm.4598

Selby, D., & Creaser, R. A. (2001). Re-Os Geochronology and Systematics in Molybdenite from the Endako Porphyry Molybdenum Deposit, British Columbia, Canada. *Economic Geology*, *96*(1), 197–204. https://doi.org/10.2113/gsecongeo.96.1.197

Selby, D., & Creaser, R. A. (2004). Macroscale NTIMS and microscale LA-MC-ICP-MS Re-Os isotopic analysis of molybdenite: Testing spatial restrictions for reliable Re-Os age determinations, and implications for the decoupling of Re and Os within molybdenite. *Geochimica et Cosmochimica Acta*, *68*(19), 3897–3908. https://doi.org/10.1016/j.gca.2004.03.022

Selby, D., Kelley, K. D., Hitzman, M. W., & Zieg, J. (2009). Re-Os sulfide (bornite, chalcopyrite, and pyrite) systematics of the carbonate-hosted copper deposits at Ruby Creek, southern Brooks Range, Alaska. *Economic Geology*, *104*(3), 437–444. https://doi.org/10.2113/gsecongeo.104.3.437

Shen, J. J., Papanastassiou, D. A., & Wasserburg, G. J. (1996). Precise Re-Os determinations and systematics of iron meteorites. *Geochimica et Cosmochimica Acta*, *60*(15), 2887–2900. https://doi.org/10.1016/0016-7037(96)00120-2

Shirey, S. B., & Walker, R. J. (1995). Carius Tube Digestion for Low-Blank Rhenium-Osmium Analysis. *Analytical Chemistry*, *67*(13), 2136–2141. https://doi.org/10.1021/ac00109a036

Sibson, R. H., Moore, J. M. M., & Rankin, A. H. (1975). Seismic pumping—a hydrothermal fluid transport mechanism. *Journal of the Geological Society*, *131*(6), 653–659. https://doi.org/10.1144/gsjgs.131.6.0653

Smith, E. M., Ni, P., Shirey, S. B., Richardson, S. H., Wang, W., & Shahar, A. (2021). Heavy iron in large gem diamonds traces deep subduction of serpentinized ocean floor. *Science Advances*, *7*(14). https://doi.org/10.1126/sciadv.abe9773

Smoliar, M. I., Walker, R. J., & Morgan, J. W. (1996). Re-Os Ages of Group IIA, IIIA, IVA, and IVB Iron Meteorites. *Science*, *271*(5252), 1099–1102. https://doi.org/10.1126/science.271.5252.1099

Snow, J. E., & Reisberg, L. (1995). Os isotopic systematics of the MORB mantle: results from altered abyssal peridotites. *Earth and Planetary Science Letters*, *133*(3–4), 411–421. https://doi.org/10.1016/0012-821x(95)00099-x

Spangenberg, J. E., Saintilan, N. J., & Palinkaš, S. S. (2022). Safe, accurate, and precise sulfur isotope analyses of arsenides, sulfarsenides, and arsenic and mercury sulfides by conversion to barium sulfate before EA/IRMS. *Analytical and Bioanalytical Chemistry*, *414*(6), 2163–2179. https://doi.org/10.1007/s00216-021-03854-y

Stein, H. J., Markey, R. J., Morgan, J. W., Hannah, J. L., & Scherstén, A. (2001). The remarkable Re–Os chronometer in molybdenite: how and why it works. *Terra Nova*, *13*(6), 479–486. https://doi.org/10.1046/j.1365-3121.2001.00395.x

Stein, H. J., Scherstén, A., Hannah, J., & Markey, R. (2003). Subgrain-scale decoupling of Re and 187Os and assessment of laser ablation ICP-MS spot dating in molybdenite. *Geochimica et Cosmochimica Acta*, *67*(19), 3673–3686. https://doi.org/10.1016/s0016-7037(03)00269-2

Stein, H. J., Zimmerman, A., Ilmen, S., Oberthür, T., Maacha, L., & Zouhair, M. (2021). Molybdenite under Stress: Dating the Contrarian Bou Azzer Co-Ni-As Deposit, Morocco. *Goldschmidt2021 Abstracts*. https://doi.org/10.7185/gold2021.8184

Takahashi, Y., Uruga, T., Suzuki, K., Tanida, H., Terada, Y., & Hattori, K. H. (2007). An atomic level study of rhenium and radiogenic osmium in molybdenite. *Geochimica et Cosmochimica Acta*, *71*(21), 5180–5190. https://doi.org/10.1016/j.gca.2007.08.007

Tourneur, E., Chauvet, A., Kouzmanov, K., Tuduri, J., Paquez, C., Sizaret, S., Karfal, A., Moundi, Y., & El Hassani, A. (2021). Co-Ni-arsenide mineralisation in the Bou Azzer district (Anti-Atlas, Morocco): Genetic model and tectonic implications. *Ore Geology Reviews*, *134*, 104128. https://doi.org/10.1016/j.oregeorev.2021.104128

Triantafyllou, A., Berger, J., Baele, J.-M., Bruguier, O., Diot, H., Ennih, N., Monnier, C., Plissart, G., Vandycke, S., & Watlet, A. (2018). Intra-oceanic arc growth driven by magmatic and tectonic processes recorded in the Neoproterozoic Bougmane arc complex (Anti-Atlas, Morocco). *Precambrian Research*, *304*, 39–63. https://doi.org/10.1016/j.precamres.2017.10.022

Vermeesch, P. (2018). IsoplotR: A free and open toolbox for geochronology. *Geoscience Frontiers*, *9*(5), 1479–1493. https://doi.org/10.1016/j.gsf.2018.04.001

Völkening, J., Walczyk, T., & G. Heumann, K. (1991). Osmium isotope ratio determinations by negative thermal ionization mass spectrometry. *International Journal of Mass Spectrometry and Ion Processes*, *105*(2), 147–159. https://doi.org/10.1016/0168-1176(91)80077-z

Wendt, J. (1985). Disintegration of the continental margin of northwestern Gondwana: Late Devonian of the eastern Anti-Atlas (Morocco). *Geology*, *13*(11), 815–818.

Wendt, J. (2021). Middle and Late Devonian sea-level changes and synsedimentary tectonics in the eastern Anti-Atlas (Morocco). *Journal of African Earth Sciences*, *182*, 104247. https://doi.org/10.1016/j.jafrearsci.2021.104247

Wendt, J., & Belka, Z. (1991). Age and depositional environment of upper devonian (early Frasnian to early famennian) black shales and limestones (Kellwasser facies) in the eastern Anti-Atlas, Morocco. *Facies*, *25*(1), 51–89. https://doi.org/10.1007/bf02536755

Williams-Jones, A. E., & Vasyukova, O. V. (2022). Constraints on the Genesis of Cobalt Deposits: Part I. Theoretical Considerations. *Economic Geology*, *117*(3), 513–528. https://doi.org/10.5382/econgeo.4895

Wise, S. A., & Watters, R. L. (2011). *Reference Material 8599 Henderson Molybdenite* (p. 30). National Institute of Standards and Technology, Report of Investigation.

Wu, K., Zhang, L., Yuan, H., Sun, W., Deng, J., Zartman, R. E., Guo, J., Bao, Z., & Zong, C. (2021). Boron, arsenic and antimony recycling in subduction zones: New insights from interactions between forearc serpentinites and CO2-rich fluids at the slab-mantle interface. *Geochimica et Cosmochimica Acta*, *298*, 21–42. https://doi.org/10.1016/j.gca.2021.01.039

Ziegler, W., & Sandberg, C. A. (1990). The Late Devonian standard conodont zonation. *Senckenbergische Naturforschende Gesellschaft*, *121*, 1–115.

SUPPLEMENTARY MATERIALS

Supplementary Materials

Download: https://ajsonline.org/article/91400-the-world-s-highest-grade-cobalt-mineralization-at-bou-azzer-associated-with-gondwana-supercontinent-breakup-serpentinite-and-kellwasser-hydrocarbon/attachment/190371.pdf